Acta Neuropathologica Communications

RESEARCH

Open Access

Spatial characterisation of TREM2 expression in actively demyelinating multiple sclerosis lesions supports its key roles in lipid metabolic pathways

Yvonne A Aguirre Candia[1†], Ekaterina Aladyeva[2†], William J Boyden[1], Bryan Bollman[3], Lara Rogerson-Wood[1], Danielle S Davies[4,5], Andrew J Affleck[4,5], Michael E Buckland[4,5], Oscar Harari[2], Laura Piccio[1,5*] and Claire S Goldsbury[1,5*]

Abstract

Reactive macrophages and microglia are predominant myeloid cell types in demyelinating multiple sclerosis (MS) lesions in the central nervous system (CNS). Triggering receptor expressed on myeloid cells-2 (TREM2) promotes clearance of myelin debris, supporting remyelination in preclinical models. However, the relevance of TREM2 in people with MS is less understood. We evaluated TREM2 expression and function in autopsy CNS tissues from individuals with and without MS. Spatial transcriptomics and gene co-expression network analysis revealed *TREM2* expression in chronic active MS lesioned white matter, where it was localised to glial cell rich clusters associated with lipid and cholesterol metabolism, cellular heat acclimation pathways, and regulation of oligodendrocyte precursor migration and differentiation. Immunofluorescence analysis confirmed that TREM2 was highly expressed in actively demyelinating MS white matter lesions (active lesion centres and chronic active lesion rims). In these areas, TREM2 was found in reactive microglia, perivascular macrophages, and infiltrating parenchymal macrophages. Similarities were observed between perilesional white matter (PLWM) and chronic active lesion rims, including presence of TREM2+ reactive microglia, which were rare in normal appearing white matter (NAWM). TREM2+ cells co-expressed microglia/macrophage markers Iba1, MHC class II, MS4A4A, CD68 and/or CD163, and PLIN2, a lipid storage marker. Almost all TREM2+ cells in active demyelinating white matter were also PLIN2+, while these cells were absent in NAWM. Abluminal TREM2+ PLIN2+ CD163+ vessel macrophages were particularly prominent in actively demyelinating MS white matter where they may play important roles in lipid metabolism and storage in the context of active demyelination. These findings highlight the involvement of TREM2 on both resident and

[†]Yvonne Aguirre Candia and Ekaterina Aladyeva are equal first authors.

*Correspondence:
Laura Piccio
Laura.piccio@sydney.edu.au
Claire S Goldsbury
claire.goldsbury@sydney.edu.au

Full list of author information is available at the end of the article

infiltrating myeloid cell populations in response to the demyelinating insult within MS lesions that may directly or indirectly impact local oligodendrocyte myelination capacity and neuroprotection.

Keywords Demyelination, Multiple sclerosis, Spatial transcriptomics, Triggering receptor expressed on myeloid cells 2 (TREM2), Perilipin 2 (PLIN2), Neuroimmunology

Introduction

Multiple sclerosis (MS) is characterised by demyelination and axonal injury in the central nervous system (CNS), driven by an autoimmune response. Immune activation and the breakdown of the blood–brain barrier occur early in MS, with infiltration of inflammatory cells including phagocytic macrophages into the CNS. Some of these cells take up and digest myelin, lipid and protein products within active focalised CNS lesions [1, 2]. Demyelination, and if severe, neuro-axonal loss, results in varying neurological impairments depending on lesion location. Resolution of immune activation, remyelination and neurological recovery can occur, but often MS becomes an ongoing chronic condition marked by superimposed relapses with the formation of new lesions, followed by remissions in relapsing–remitting MS (RRMS). Most cases advance to a progressive disease marked by the degeneration of demyelinated axons, leading to permanent injury and clinical progression (secondary progressive MS–SPMS; or in 10–15% of cases, primary progressive MS–PPMS, where the disease is progressive right from the beginning). Progressive MS correlates with the increasing presence of "slowly expanding", chronically active demyelinated lesions that each have a relatively hypocellular demyelinated centre, with a rim of iron-laden reactive microglia/macrophages associated with ongoing demyelination [3–5].

Myeloid cells in the normal CNS comprise microglia in the parenchyma and border-associated macrophages in the meninges, choroid plexus, and perivascular spaces of grey and white matter [6]. Infiltrates of monocytes differentiate and colonise MS lesions, intermingling with resident microglia and perivascular macrophages (PVMs), and express overlapping genes [2]. This immune-mediated influx of phagocytic macrophages into the CNS has been suggested to be highly damaging and representative of an initial cause of demyelination and disability in MS, although these cells may also exert protective functions in their phagocytic and anti-inflammatory capacities [7]. Evidencing dual capacities, "disease-associated microglia" (DAM) genetic signatures are activated in microglia/PVMs in response to CNS injury, and these enable processes required for the tissue repair and renewal functions of these cells [8].

TREM2 (triggering receptor expressed on myeloid cells-2) is an important DAM activation receptor in human and mouse microglia [8, 9]. Consistent with a neuroprotective role of TREM2, in the cuprizone model of demyelination, TREM2 deficient (Trem2−/−) mice have broad defects in microglial responses to myelin damage, including defective activation, reduced proliferation, reduced levels of lipoprotein lipase (LPL) (a key enzyme implicated in lipid transport and metabolism) and impaired myelin clearance, resulting in greater CNS demyelination and neurological deficit in this model [10–12]. Elevating TREM2 in peripheral monocytes facilitates tissue repair and remyelination in experimental autoimmune encephalomyelitis (EAE) [13]. Similarly, activation of TREM2 using an agonist antibody enhanced remyelination in the cuprizone model by promoting myelin debris clearance, a critical step to allow remyelination, intracellular lipid metabolism and degradation [12], whereas blocking TREM2 in microglia had the opposite effect [14].

TREM2 is implicated in lipid droplet (LD) biogenesis [15]. LDs are lipid-storing organelles with a core of esterified cholesterol and fatty acids, that maintain lipid homeostasis and prevent lipotoxicity [16]. *Trem2*−/− mice showed defective LD formation, as free cholesterol could be internalised but not metabolised [17]. The perilipin (PLIN) family is the most abundant LD-coating protein, of which PLIN2 is the most prevalent in the CNS, and it is expressed by microglia, neurons, and astrocytes [18]. TREM2 function has also been linked to the family of MS4A proteins, in particular MS4A4A, which modulates receptor ectodomain shedding that releases soluble TREM2 [19]. Peripheral macrophages express MS4A4A [20], which may be involved in polarising to an anti-inflammatory phenotype with phagocytic functions, implicating TREM2 and MS4A4A in reparative processes [21, 22]. MS4A4A has been implicated in lipid metabolism and immune activation in microglia in Alzheimer's disease brains and in preclinical models [23, 24], but its expression has not been characterised in MS lesions.

Elevated *TREM2* mRNA is observed in demyelinating MS lesions in humans, and soluble TREM2 is increased in the cerebrospinal fluid (CSF) of people with MS [25, 26]. However, the timing and spatial distribution of TREM2 expression in MS is not well characterised. Here we characterise TREM2 expression in different types of myeloid cells (microglia, macrophages and PVMs), and in distinct tissue areas—demyelinating, perilesional (PLWM) and normal appearing white matter (NAWM) in MS and control tissues using spatial transcriptomics and immunofluorescence. Our data links TREM2 to active

cholesterol lipid metabolism and storage that occurs in response to demyelination in MS.

Materials and methods

Human MS and control tissue

Provision of control and MS tissue sections was approved by the University of Sydney human ethics committee (2020/HE000149) and by peer-reviewed tissue request processes of the Multiple Sclerosis Australia Brain Bank (MSABB), Sydney Brain Bank (SBB), NSW Brain Tissue Resource Centre (NSWBTRC) and the Neuroinflammatory Disease Tissue Repository at Washington University St. Louis. Tissues were fixed with 10% formalin (at the time of autopsy), embedded in paraffin (formalin-fixed paraffin-embedded; FFPE) and sectioned at 5 µm. Neuropathological characterisation was performed independently by brain bank/repository neuropathologists and confirmed by our group upon receipt of the tissue. Clinical characterisation, case demographics, CNS regions, lesion types, and the associated brain bank are summarised in Table 1.

MSABB characterisation of tissue blocks was performed by Oil Red O (ORO) staining, Luxol Fast Blue (LFB) staining, CD68 and Myelin Basic Protein (MBP) immunohistochemistry. Neuroinflammatory Disease Tissue Repository at Washington University characterised tissue blocks using Solochrome cyanine [27] or LFB staining to visualise myelin and lesions, and MHC class II immunohistochemistry to visualise reactive microglia/macrophages and to classify the lesion activity. HRP goat anti-mouse IgG Polymer Kit (Vector, MP7452) and ImmPACT DAB Substrate Kit (Vector, SK-4105) were used to expose the HRP.

Active white matter lesions were characterised by demyelination and abundant ORO+ lipid-laden macrophages throughout the lesion. In addition, elevated CD68 or MHC class II, as well as CD163 immunolabelling, was characteristic of reactive microglia/macrophages in areas of active demyelination [1]. Chronic active lesions contained ORO+ lipid-laden (and MHC class II+/CD68) microglia/macrophages in a distinctive rim around a hypocellular demyelinated lesion centre. Chronic inactive lesions contained demyelinated centres with no ORO+ cells, and remyelinating lesions contained a patchy-MBP immunolabelled core with few ORO+ cells. Tissue blocks/sections could contain one or more lesion types. Normal-appearing white matter (NAWM) blocks contained no visible lesions. Controls had no evidence of neurological diseases.

Preparation of transcriptomic slides and NovaSeq 6000 spatial transcriptomic library

Two independent demyelinating chronic active lesions in the hippocampus/parahippocampal gyrus were selected for spatial transcriptomic analysis: MS13C, containing a rim of hypertrophic MHC class II+ microglia characteristic of chronic active lesions, and MS15A. The MS13C and MS15A tissues were characterised by a neuropathologist at the Neuroinflammatory Disease Tissue Repository at Washington University, St. Louis. The tissues underwent histopathological characterisation, where chronic active lesion rims surrounding hypocellular demyelinated cores were identified in both tissues using myelin stains and immunohistochemistry. We note that the two lesions come from two individuals and, although both are confirmed chronic active lesions, they are not identical. The MS13C section contained more activation in the rim, as noted by extensive MHC class II positive microglia. MS15A contained fewer activated microglia.

FFPE sections were prepared using the 10X Genomics Visium CytAssist Spatial Gene Expression for FFPE, Human Transcriptome, 11 mm, 2 rxns kit (PN-1000522). Libraries were tagged with indexes from the Dual Index Kit TS Set A, 96 rxns kit (PN-1000251). The area captured was 11 × 11 mm. The library concentration of each sample was amplified and determined through qPCR utilising the KAPA Library Quantification Kit in accordance with the manufacturer's protocol (KAPA Biosystems/Roche) to produce cluster counts appropriate for the Illumina NovaSeq6000 instrument. Normalised libraries were sequenced on a NovaSeq6000 S4 Flow Cell using the XP workflow and a 28x10x10x151 sequencing recipe according to manufacturer protocols. Target sequencing depth was determined prior to pooling, and samples were pooled in ratios based on the targeted depth. The final library sizes were 236 bp for MS15A and 237 bp for MS13C.

Spatial transcriptomics analysis

We aligned 10X Genomics Visium sequences using SpaceRanger v2.0.0, employing the refdata-gex-GRCh38-2020-A as a reference of the human transcriptome downloaded from the 10X Genomics site. The resulting count matrices and corresponding spatial information were pre-processed using Seurat v4 [28]. Spots that did not contain the detected tissue and spots that were not part of the hippocampus were removed using visual inspection. The mean number of detected genes for selected spots contained 2747 and 2582 genes for samples MS13C and MS15A, respectively. Gene expression was normalised using the SCTransform function to remove the technical effects of sequencing depth. Samples were then integrated using 2000 features, and principal component analysis was performed on the integrated matrix. The first 12 principal components were employed as the inputs for the UMAP dimensionality reduction. Using unsupervised clustering, we identified 19 distinct spatial transcriptomic clusters with a clustering resolution of

Table 1 Demographic and clinical characteristics of autopsy control and MS cases

Case[a]	Type of MS (EDSS)[c]	Sex/ Age	MS duration	PMI (hrs)	Cause of death	Brain region[e]	Lesion type	Treatment
C1	n.a.	F/35	NA	13	Metastatic colon cancer	Hippocampus	n.a	n.a
C2	n.a.	M/34	NA	12	Acute myelogenous leukemia	Spinal cord	n.a	n.a
C3	n.a.	M/73	NA	3	Cardiac arrest	Hippocampus	n.a	n.a
C4	n.a.	F/69	NA	43	Sepsis	Medulla	n.a	n.a
C5	n.a.	M/41	NA	24	Heart failure	Hippocampus	n.a	n.a
C6	n.a.	F/92	NA	31	Chronic obstructive pulmonary disease	Superior FrontalCortex	n.a	n.a
C7	n.a.	M/69	NA	16	Cardiac arrest	Superior Frontal Cortex	n.a	n.a
C8	n.a.	F/85	NA	23	Pneumonia	Superior Frontal Cortex	n.a	n.a
MS1	PPMS	M/73	15.6	25.5	Gangrene Left foot (+ peripheral vascular disease, IHD, MS)	Parietal Cortex Occipital Cortex Frontal Cortex	Active (A) Remyelinating (B) NAWM (C)	Not available
MS2	MS[d]	F/44	0.3	6	MS	Periventricular Periventricular Superior Temporal Cortex	Active (A) Active (B) NAWM (C)	Not available
MS3[b]	SPMS & PML	M/41	13.6	17	MS (+ PML)	Occipital Cortex Inferior Frontal Cortex Frontal Cortex Posterior Cingulate Cortex Basal Ganglia	Active (A) Active & Remyelinating (B) Remyelinating (C) Chronic Inactive (D) Active & PML (E)	Not available
MS4	RRMS	F/36	9	80	MS	Deep WM Periventricular Inferior Parietal Cortex	Active (A) Active & Remyelinating (B) NAWM (C)	Not available
MS5	SPMS	F/55	26	7	Urosepsis	Anterior Cingulate Cortex Frontal Cortex	Active & Remyelinating (A) NAWM (B)	Not available
MS6	SPMS	F/50	18	35	Aspiration pneumonia (+ severe MS, cardiac failure)	Pons Periventricular Parietal Cortex	Active & Remyelinating (A) Remyelinating (B) NAWM (C)	Not available
MS7	SPMS	F/68	33.5	15	Hypoxic brain injury, upper airway obstruction, MS	Periventricular Occipital Cortex Anterior Cingulate Cortex	Active & Chronic inactive (A) Remyelinating (B) NAWM (C)	Not available
MS8	SPMS	F/47	26	21	Urosepsis, MS	Frontal Cortex Frontal Cortex Frontal Cortex	Active & Chronic inactive (A) Remyelinating (B) NAWM (C)	Not available
MS9	SPMS	F/82	60	68	Atherosclerotic and hypertensive cardiovascular disease (+ morbid obesity)	Anterior Cingulate Cortex Anterior Cingulate Cortex Frontal Cortex	Remyelinating (A) Remyelinating (B) NAWM (C)	Not available
MS 10	RRMS	M/61	1.6	22	Concomitant MS and primary lateral sclerosis	Cingulate Cortex Cingulate Cortex Occipital Cortex Temporal Cortex	Chronic Active (A) Chronic Inactive (B) Remyelinating (C) NAWM (D)	Not available
MS 11	PPMS	M/35	10	10	Unknown	Midbrain	Chronic Active (A)	No treatment for MS
MS 12	SPMS (EDSS = 9)	F/45	7	5	Respiratory Failure	Pons	Active (A)	Intermittent IV Steroids

Table 1 (continued)

Case[a]	Type of MS (EDSS)[c]	Sex/ Age	MS duration	PMI (hrs)	Cause of death	Brain region[e]	Lesion type	Treatment
MS 13	SPMS (EDSS = 9)	F/54	22	8	Pneumonia	Medulla Frontal Cortex Hippocampus	Chronic Active (A) Chronic Active (B) Chronic Active (C)	Not reported
MS 14	SPMS	M/60	14	9	Respiratory Failure	Pons	Chronic Active (A)	Not Reported
MS 15	SPMS (EDSS = 7)	F/54	17	7	Pneumonia	Hippocampus Medulla	Chronic Active (A) Active (B)	IFNbeta & Glatiramer Acetate
MS 16	SPMS (EDSS = 7)	F/50	13	20	Unknown	Thoracic Spinal Cord	Active (A)	Fingolimod
MS 17	Unknown (EDSS = 7)	F/66	32	29	Unknown	Lumbar Spinal Cord	Active (A)	IFNb1a & intermittent steroids

[a]The Neuroinflammatory Disease Tissue Repository at Washington University, St. Louis, provided C1–5 and MS11–17; Sydney Brain Bank provided C6 and C8; NSW Brain Tissue Resource Centre provided C7; and Multiple Sclerosis Australia Brain Bank provided all other sections

[b]Case MS3 was diagnosed with PML, and no blocks from this case were included in the MS group for analysis

[c]EDSS refers to the disability around the time of death, and it is reported only when available

[d]This case had a very rapid clinical course, and the person was not defined clinically as relapsing or progressive

[e]For cerebral cortex areas, the subcortical white matter was evaluated

F = female, M = male, n.a. = not applicable, PPMS = Primary Progressive MS, SPMS = Secondary Progressive MS, RRMS = Relapsing–Remitting MS, DoD = Duration of disease from diagnosis, PMI = post-mortem interval, NAWM = Normal-appearing white matter, PML = Progressive multifocal leukoencephalopathy, IHD = ischemic heart disease, EDSS = Expanded disability status scale

0.8. To characterise these clusters, a reference single-cell RNA-seq dataset from patients with MS was integrated [29] to label the clusters with the main cell types. For the annotation of hippocampal histological areas, we integrated a second reference single-nuclei RNA-seq dataset [30], which included detailed annotations of different hippocampal subregions. Following the Seurat integration workflow, both datasets were integrated using the "FindTransferAnchors" and "TransferData" functions with default parameters for the SCTransformed datasets.

Cell abundance estimation

Spot transcriptomic data was deconvolved using Cell2Location [31] to calculate the percentage of the most representative CNS cell types. Single-cell data from the human brain was used as a reference to capture the chronic active MS lesion transcriptomics [32]. Genes from the reference dataset that were not expressed in the samples were excluded. We estimated the reference signatures using a Negative Binomial regression model trained from the Cell2Location package for 250 epochs with a batch size of 2500 cells without a validation dataset. The sampled variable ("NBB_case") was used as a covariate for the technical batch correction. The Cell2Location training model was used to perform cell abundance calculations using the following Cell2Location recommended hyperparameters: N_cells_per_location = 30 and detection_alpha = 200.

Weighted gene co-expression network analysis

Weighted gene co-expression network analysis (WGCNA) was performed for each sample individually using the package hdWGCNA [33]. Before running WGCNA, samples were reprocessed following the above procedure (spatial transcriptomics analysis). Only genes expressed in at least 5% of the spots were retained for analysis. We used "MetaspotsByGroups" and "NormalizeMetacells" for each integrated cluster to aggregate the spots in the metacells. Soft-power thresholds 10 and 8 were picked for MS13C and MS15A to remove weak connections between genes in correlation matrices. Module eigengenes and eigengene-based connectivity were found using functions "ModuleEigengenes" and "ModuleConnectivity" with default parameters. To determine the association of modules with integrated clusters, we first found cluster-specific markers using the Seurat function "FindAllMarkers" and ran Fisher's exact test for overlap between module hub genes and differentially expressed genes in clusters. For correlation analysis between Cell2Location estimated proportions and identified modules, we performed a Pearson correlation test using the hdWCGNA function "ModuleTraitCorrelation." Enrichment analysis was implemented with the "RunEnrichr" function against two Enrichr [34] gene set databases, "GO_Biological_Process_2023" and "KEGG_2021_Human", using the top 100 genes from each module. Only terms with FDR-adjusted p-values less than 0.05 were selected for reporting. We first filtered out spots with highly expressed hub genes from the corresponding

glial-associated modules for each sample to find submodules. We repeated the same steps from the WCGNA procedure on selected spots.

Immunofluorescence

Sections were dewaxed, followed by antigen retrieval in citrate buffer (20 min, 110 °C). After blocking (5% horse serum, 0.1% Saponin in PBS, 1 h), slides were incubated overnight at 4 ℃ with primary antibodies (Table 2) in PBS, then rinsed in PBS, and incubated with fluorescent conjugated Alexa Fluor (AF) secondary antibodies (AF488, AF555, AF647; Table 2) in PBS for 1 h at room temperature. DAPI (1 µg/mL) was added for 2 min at the end of the secondary antibody incubation. Slides were rinsed in PBS, mounted with Prolong Gold (Thermofisher, USA, P36930), and set for > 48 h before imaging. Negative controls for all tissue blocks were conducted by omitting primary antibodies. An isotype goat IgG control was performed for the polyclonal goat anti-TREM2 (AF1828) immunofluorescence.

Microscopy

Lesions were identified using histopathology slides of nearby sections in the same block provided by the brain banks or repositories. Slides were imaged using the Olympus VS120 scanner at the Sydney Microscopy and Microanalysis (SMM) Facility at the University of Sydney and the Hamamatsu NanoZoomer 2.0-HT System in the Alafi Neuroimaging Laboratory at Washington University in St. Louis, with 20× objectives. Higher-resolution imaging of histology slides was performed using the Leica DM6000 microscope at the SMM facility at the University of Sydney.

Immunofluorescence images were generated using the Nikon C2 confocal microscope equipped with three standard PMTs (DAPI/Cy5, FITC and TRITC) at the SMM facility at the University of Sydney. Three images were captured from each area of interest in the section—for example, three in the chronic active centre, three in the chronic active rim and three in the peri-lesional white matter (PLWM). Sequential scans were used for image capture utilising laser wavelengths of 405 µm, 488 µm, 561 µm, and 640 µm, with a scanner zoom of 1.00 and a one-way scan direction. Laser settings were optimised and kept the same for all imaging. Images 1024 × 1024 pixels (312.39 × 312.39 µm) in 4-step z-stacks (total thickness between 1–1.7 µm) were acquired using a Plan Apo 40x, NA = 0.95 objective. Higher-resolution 1024 × 1024 pixels (126.04 × 126.04 µm) images were captured using a Plan Apo 100× Oil NA = 1.45 objective, and 6-step z-stacks.

Table 2 Primary and secondary antibodies

Primary antibody (Clonality)	Reactivity	Source (Cat#)	Dilution
Goat anti-human TREM2 (Polyclonal)	Microglia/macrophages, Endothelium	R&D Systems, USA (AF1828)	1:200
Rabbit anti-human Iba1/AIF1 (Polyclonal)	Microglia/macrophages	Wako, Japan (019-19741)	1:100
Mouse anti-human CD163 (Monoclonal)	(Perivascular) macrophages/rare microglia	Abcam, UK (ab201461)	1:100
Mouse anti-human CD68 (Monoclonal)	Microglia/macrophages	Agilent, USA (M087601-2)	1:75
Mouse anti-human MHC class II (Monoclonal)	Microglia/macrophages	Invitrogen, USA (MA1-25914)	1:50
Rabbit anti-human ADRP/Perilipin 2 (Polyclonal)	Lipid Droplets	United Bioresearch, Australia (15294-1-AP)	1:50
Rabbit anti-human MS4A4A (Polyclonal)	Macrophages/rare microglia	Novus, USA (NBP1-86542)	1:100
Rabbit anti-human TMEM119 (Polyclonal)	Microglia	Sigma-Aldrich, USA (HPA051870)	1:1000
Rat anti-human/mouse TREM2 (Monoclonal)	Nonspecific	R&D Systems, USA (MAB17291)	1:200
Mouse anti-human Iba1 (Monoclonal)	Microglia	Sigma-Aldrich, USA (MABN92)	1:50
Rabbit anti-human TREM2 (Polyclonal)	Nonspecific	Cusabio, US (CSB-PA024405LA01HU)	1:100
Rabbit anti-human TREM2 (Polyclonal)	Nonspecific	ProSci, USA (13-679)	1:100
Rabbit anti-human TREM2 (Polyclonal)	Endothelium	Invitrogen, USA (PA5-87933)	1:100
Rabbit anti-human TREM2 (Monoclonal)	Nonspecific	Cell Signalling, USA (D8I4C)	1:100
Mouse anti-human TREM2	Microglia	N/A (21E10)	1:200
Mouse anti-human TREM2	Microglia	N/A (T22)	1:200
Goat IgG Control	Isotype control	R&D Systems, USA (AB-108-C)	1:200
Secondary antibody (Alexa Fluor Conjugate)	**Reactivity**	**Source (Cat#)**	**Dilution**
Donkey anti-rabbit (647)	Anti-rabbit primary antibodies	Invitrogen, USA (A-32795)	1:200

Table 2 (continued)

Secondary antibody (Alexa Fluor Conjugate)	Reactivity	Source (Cat#)	Dilution
Donkey anti-goat (555)	Anti-goat primary antibodies	Invitrogen, USA (A-21432)	1:200
Donkey anti-mouse (488)	Anti-mouse primary antibodies	Invitrogen, USA (A-32766)	1:200

Image analysis

TREM2+, Iba1+ and CD163+ PVMs, parenchymal macrophages and microglia in NAWM and MS lesions (active, chronic active, chronic inactive and remyelinating lesions) were quantified from confocal 312.39 × 312.39 µm maximum projection images.

Cell densities

In maximum intensity projection images of TREM2, Iba1, and CD163 triple-labelled sections, single, double and triple-labelled cells were counted using Fiji/ImageJ. All DAPI-stained nuclei were identified, followed by those cells positive for Iba1, CD163 or TREM2 labelling. Three images from each area of interest (lesion centre, PLWM, rim, NAWM) per block were analysed, and the proportions of single, double and triple labelled cells were determined.

Cell counts were performed blinded to the pathological status of the imaged tissue and by a different researcher from the one who performed the immunolabelling and microscopy. ImageJ/FIJI was used to measure cell counts in maximum intensity projections. To determine the total number of cells, all DAPI cell nuclei of parenchymal, non-vessel-associated cells were counted. The resultant DAPI nucleus count overlay was then used as the scaffold for determining the proportion of CD163+ /Iba1+ cells in the image. DAPI cell nuclei demarcations (as delineated by the overlay) without clear associated CD163 or Iba1 labelling were deleted from the overlay, resulting in a new CD163/Iba1+ cell count overlay. A thresholding step was included before determining TREM2+ cell count overlays. For this, an assessment of the background intensity of each image was first undertaken using the merged CD163/Iba1 channels to outline cell-negative areas in each image (capturing at least 1/3 of the imaged area). This selection was applied to the TREM2 channel to determine the background fluorescence mean and standard deviation in the AF555 channel. The minimum display value for each image was set to this calculated mean plus one standard deviation, whilst ensuring the maximum display value was set to 4095 to capture the entire pixel intensity range for consistency between images. The associated CD163/Iba1 positive nuclei count overlay was then applied to the thresholded TREM2 channel. All points without a TREM2 positive perinuclear ring, or at least 50% of the cell surface as TREM2+, were subtracted, resulting in the TREM2 positive cell count overlay. Negative control images (omitted TREM2 primary antibody but included CD163 or Iba1 primary antibodies and all secondary antibodies) were included and processed in the same manner as the experimental images to ensure the validity of the image analysis procedure for detecting TREM2-positive cells. Counts for each set of multipoint overlays (DAPI+, CD163/Iba1+, and TREM2+) were obtained for each image. The same approach was used to measure the proportions of CD68, TMEM119, MS4A4A, PLIN2, MHC class II, and TREM2-positive cells in different images.

Immunofluorescence intensity analysis

Confocal immunofluorescence images from 6 independent blocks, each of NAWM (control and MS), active, chronic active, and remyelinating lesions, were used to measure the pixel intensity per cell. From each image, the pixel intensity of up to 20 triple-labelled cells was measured in each channel (60 cells per case for each region of interest). Three non-labelled areas without cells were measured to determine the background intensities of AF488, AF555 and AF647 channels. The total intensity per cell was calculated by multiplying the mean pixel intensity by the area and subtracting the background area intensity for a given channel. The size of the measured area ranged from 64.032 to 294.658 μm^2 to capture the entire cell and the least amount of background area possible. Cell intensities in different regions of the same tissue section were compared, for example, perilesional, rim and lesion centre areas. Cell intensities in NAWM were measured by using 12 independent tissue Sections (6 MS and 6 controls). Data was transferred into Excel, then GraphPad Prism for presentation and analysis using an ordinary one-way ANOVA and Šídák's multiple comparisons test (95% confidence interval; CI).

Results

Spatial transcriptomic analysis resolves distinct cell populations in chronic active lesions from people with progressive MS and reveals that TREM2+ cells are enriched in actively demyelinating lesion areas

To investigate the distribution of *TREM2* and gene expression networks in myeloid cell subpopulations in MS lesions, we performed spatial transcriptomic analyses on autopsy hippocampal tissues containing chronic active white matter lesions from two people with SPMS (MS13C and MS15A; Fig. 1a, Table 1). Before sequencing, adjacent serial sections of the tissues containing the lesions were immunolabeled for MHC class II (activation marker) and stained with LFB to mark actively demyelinating areas (Fig. 1b). Both cases contained focal areas of demyelination surrounded by MHC class II+ microglia/

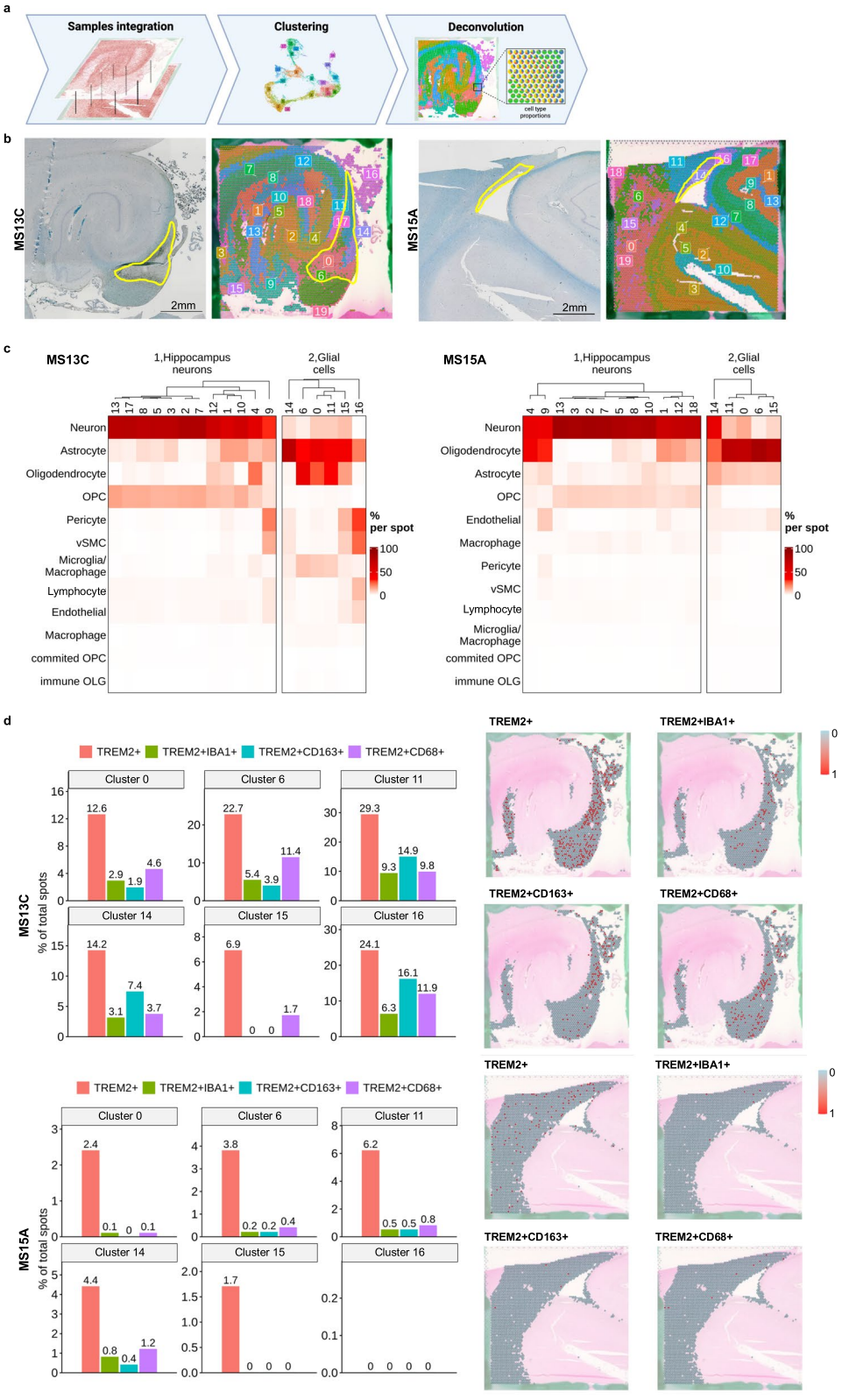

Fig. 1 (See legend on next page.)

(See figure on previous page.)

Fig. 1 Spatial transcriptomics in hippocampal tissue containing chronic active lesions from two cases (MS13C and MS15A) of secondary progressive MS. **a** Schematic of spatial transcriptomics workflow using sample integration, clustering and deconvolution functions. **b** LFB staining and MHC class II immunohistochemistry were used to identify lesioned (yellow outline) areas (2 mm scale bar; left panels). **c** Cell populations were estimated by deconvolution analysis of spatial gene expression profiles in each cluster. Clusters 0, 4, 11, 14, 15, and 16 contained a higher proportion of glial cells relative to other clusters associated with neuronal cell types in the hippocampus. **d** Quantitative analysis of spatial distributions of total *TREM2*+ spots and TREM2 in relation to selected myeloid cell markers (*CD68, CD163, IBA1*). OPC = Oligodendrocyte progenitor cell, vSMC = Vascular smooth muscle cell, OLG = Oligodendrocyte

macrophages corresponding to chronic active lesions. MS13C exhibited a rim with abundant MHC class II+ microglia/macrophages around a hypocellular demyelinated lesion centre. The rim of the MS15A chronic active lesion contained sparser MHC class II+ cells.

Spatially resolved transcriptomics was generated using 10X Visium technology, which provides transcriptome-wide expression data and spatial distributions. We initially obtained 9252 spots for MS13C and 12,893 spots for MS15A. Data cleaning and quality control preprocessing included detecting and removing spots in border areas that lacked tissue or did not correspond to hippocampal structures. We used the Seurat V4 pipeline [28] to evaluate the quality metrics of the remaining spots. All spots passed the initial quality control filtering based on the metrics suggested by the Seurat pipeline, which controls for the number of unique molecular identifiers (UMIs), genes, and mitochondrial content. After preprocessing, the datasets contained 6192 and 8724 spots for MS13C and MS15A, respectively. Cases were integrated using unsupervised clustering, and 19 distinct clusters were found; all clusters had spots in each case (Fig. 1a, b and Supplementary Table 1). Clusters 16 and 17 in MS13C, and Clusters 18 and 19 in MS15A had a significantly higher number of spots in the corresponding case and were considered case-specific (Table 3 and Supplementary Table 1). Clusters were anatomically matched to hippocampal regions and pathological areas of the MS lesion. Clusters 11 and 14 overlapped with the rim and lesion centre in MS13C and the lesion centre of MS15A. Clusters 0 and 6 were associated with the demyelinated centre and perilesional areas in MS13C, but were in distal proximity to the lesion in MS15A. Cluster 15 spots, mainly associated with MS15A, were in perilesional hippocampal areas and contained blood vessels with connected astrocytes (Table 3, Fig. 1b and Supplementary Table 1). Cluster 16 was confined to the choroid plexus and was specific to MS13C. Pathological reports and immunohistochemistry verified the absence of the choroid plexus in the MS15A tissue section, explaining the lack of Cluster 16. The remaining UMAP clusters contained neuron-specific marker genes, which were anatomically associated with hippocampal neuronal layers.

Deconvolution approaches were used to determine cellular composition for each cluster. This approach analyses the expression profile of each spot against single-cell reference data to determine the abundance of different cell types in each spot. Hippocampal cell type-specific expression profiles were determined using a reference dataset [32]. We found that Clusters 0, 6, 11, 14, 15, and 16 exhibited a high percentage of glial cells and a low percentage of neurons (Fig. 1c). Variations were observed among multiple glial cell populations when examining the average proportions of cell types within selected clusters. MS13C had more prevalent astrocytes and elevated levels of microglia, macrophages and vascular cells (endothelial cells, pericytes and vascular smooth muscle cells) compared to MS15A. In contrast, case MS15A exhibited a higher percentage of oligodendrocytes (Fig. 1c). To validate deconvolution results, we performed additional analysis by integrating a single-cell reference dataset [29] and obtained similar results.

The distribution of *TREM2*+ spots was investigated in relation to myeloid cell markers (*IBA1*, *CD163*, *CD68)*, a microglia marker (*TMEM119)* and the lipid droplet marker *PLIN2* (Fig. 1d and Supplementary Fig. 1). The spatial organisation of *TREM2*+ spots in MS13C was distinct between lesion areas; Clusters 0 and 6 (chronic-active lesion centre and perilesional areas) were enriched with TREM2+ CD68+ spots, whereas the lesion rim area in Clusters 11 and 14 contained higher proportions of TREM2+ CD163+ spots. MS13C case-specific Cluster 16 was enriched with *TREM2*+ *CD163*+ and *TREM2*+ *CD68*+ macrophages in the choroid plexus. Overall, MS15A exhibited far fewer *TREM2*+ spots compared to MS13C. The proportions of *TREM2*+ *TMEM119*+ and *TREM2*+ *PLIN2*+ spots were relatively low in both cases (Supplementary Fig. 1). This may be due to poor transcriptomic detection of the *PLIN2* transcript, as abundant PLIN2 was detected by immunofluorescence (see below). However, Cluster 11 (rim-associated cluster) in MS13C had increased *TREM2*+ *PLIN2*+ and *TREM2*+ *TMEM119*+ spots compared to Clusters 0, 6, 14, 15 and 16. This suggests that *TMEM119*+ cells, most likely microglia, contain lipid droplets in the rim but not in the lesion centre (Cluster 0) and PLWM areas (Cluster 6) (Supplementary Fig. 1). In contrast, the rim area (Cluster 11) in MS15A had no *TREM2*+ *PLIN2*+ spots, potentially indicating that the cells here are less lipid-filled or in a different reactive state.

Table 3 Summary of the anatomical and cellular characteristics of sample-specific and glial-enriched clusters in MS13C and MS15A

Cluster	Anatomical characterisation of notable clusters		Cellular characterisation of notable clusters	
	Case MS13C	Case MS15A	Case MS13C	Case MS15A
11,14	MHC class II positive rim	MHC class II positive rim	11: High proportion of astrocytes and oligodendrocytes. Moderate proportions of neurons and microglia/macrophages 14: High proportion of astrocytes. Low proportions of neurons and microglia/macrophages	11: High proportion of oligodendrocytes. Moderate proportions of neurons and astrocytes 14: High to moderate proportions of astrocytes, neurons and oligodendrocytes. Low proportions of endothelial cells and macrophages
0, 6	Demyelinated lesion centre and perilesional areas	Perilesional and distal areas	High proportion of astrocytes and oligodendrocytes. Low to moderate proportions of neurons and microglia/macrophages	High proportion of oligodendrocytes. Low to moderate proportions of neurons and astrocytes
15	Perilesional and distal areas	Perilesional and distal areas	High proportions of astrocytes. Moderate proportions of neurons, oligodendrocytes, pericytes and vascular smooth muscle	High proportions of oligodendrocytes. Moderate proportions of neurons and astrocytes
16	Choroid plexus (unique to this case)	N/A	High proportions of astrocytes, pericytes and vascular smooth muscle. Low proportions of lymphocytes and endothelium	N/A
17	Unique to this case	N/A	High proportion of neurons. Moderate proportions of oligodendrocyte precursor cells (OPCs)	N/A
18, 19	N/A	Unique to this case	N/A	18: High proportions of neurons and moderate proportions of oligodendrocytes and OPCs 19: No predictions were derived for this cluster

NAWM = Normal-appearing white matter, OPCs = oligodendrocyte precursor cells, N/A = Not applicable

Gene network analysis reveals the presence of diverse glial cell sub-populations in MS tissues

To identify additional associations with the discovered *TREM2*+ subpopulations, we employed a systems biology approach, using weighted gene co-expression network analysis (WGCNA) to identify modules of co-expressed genes that possibly share pathway functionality, illustrated in the workflow schematic (Fig. 2a). Heterogeneous glial cell populations were revealed in each tissue; thus, the WGCNA was applied to each case separately. However, we used integrated clusters as a covariate for the WCGNA algorithm to preserve their relationships with MS pathological spatial patterns. A preprocessing procedure in the WGNCA package was used to find and aggregate groups of related spots into metacells. This analysis revealed an association between the discovered co-expressed gene modules and spatial patterns of lesion areas. The algorithm identified four modules for MS13C, whereas only two modules were identified for MS15A due to differences in the tissues (Fig. 2b). Both cases contained two similar modules: the hippocampal neuronal area (module A) and the associated glial populations (module B). Two modules specific to MS13C belonged to the choroid plexus area (module C) and the meninges (module D) (Fig. 2b). We initially assessed the cellular population structure of these modules by correlating the hub genes (most-centred genes in the module graph) of the identified modules with the cellular population structure that we had identified previously for each spot. Hub genes in module B were positively correlated with the percentage of astrocytes, oligodendrocytes, and microglial cells in spots from both cases. Macrophages and immune cells were positively associated with module A in MS15A, which also contained a high abundance of neurons. In contrast, these populations were more associated with module B in MS13C. For modules C and D in MS13C, the percentages of endothelial, vascular leptomeningeal cells, and pericyte cells were correlated with module hub genes. An enrichment analysis was performed using the gene ontology database for biological processes to identify any functional associations of hub genes within the modules (Fig. 2c). The results for module A in both cases showed that it was enriched in elements associated with healthy neuronal activity (neurotransmitter secretion and signal transfer). Module B was enriched in heat acclimation-related gene expression (an indicator of reparative functions).

Next, we focused on those spots that expressed hub genes from module B more strongly and ran gene co-expression network analysis. As a result, we found four additional submodules in MS13C and three in MS15A (Fig. 3a). Enrichment analysis revealed the functional consistency of the submodules in both cases. Spots corresponding to submodule A were classified as homeostatic glial populations adjacent to healthy hippocampal neurons and oligodendrocyte precursor cells (OPCs) in both cases (Fig. 3b). In contrast, spots near the lesion core (submodule C in MS13C and submodule B in MS15A) were enriched for genes from the pathways associated with heat acclimation (Fig. 3d). These areas

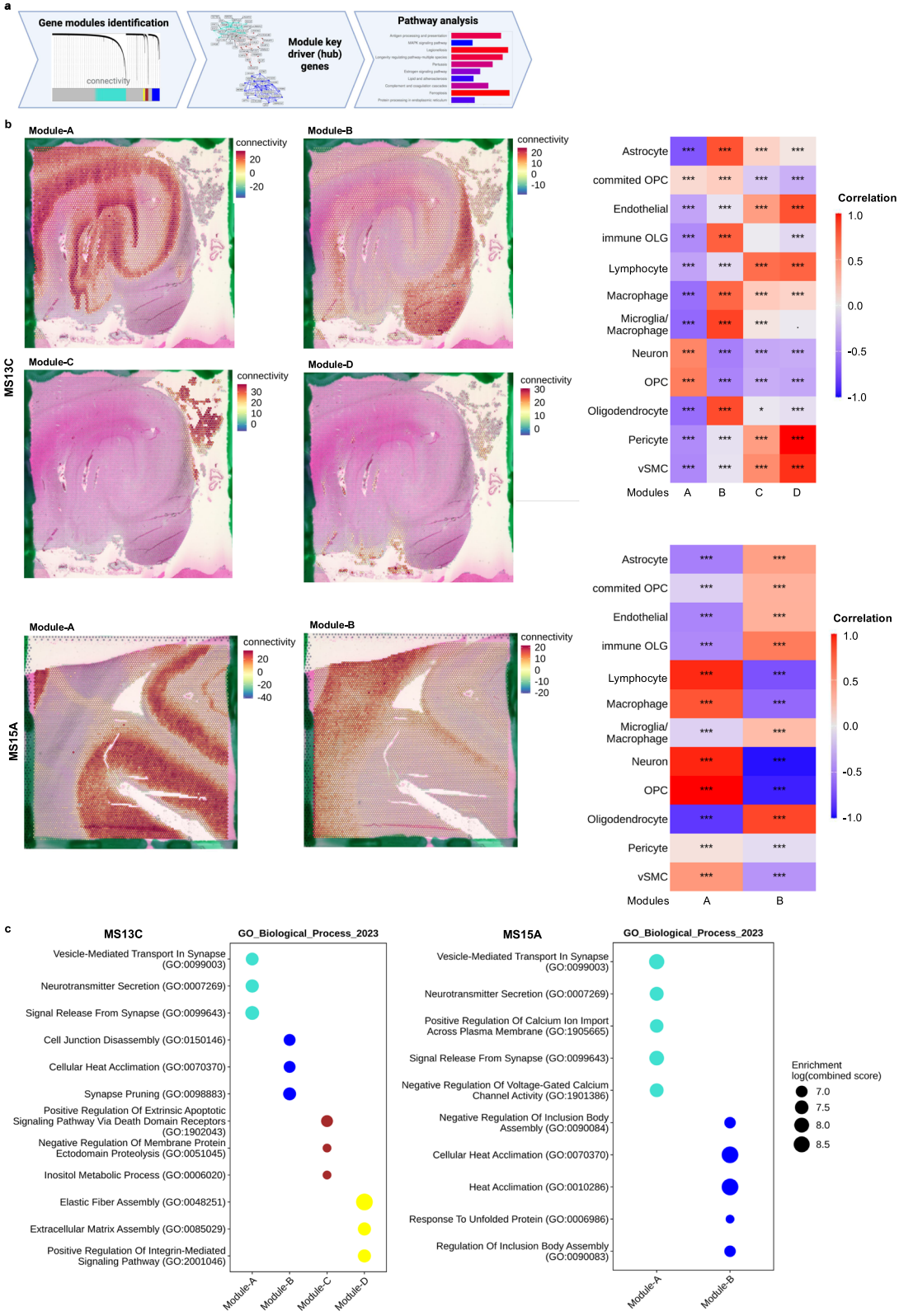

Fig. 2 Gene co-expression network analysis of glial-rich modules associated with the lesion. **a** Schematic of the weighted gene co-expression network analysis (WGCNA) workflow to identify gene modules, hub genes and relevant pathways. **b** Spatial distribution of initial modules for MS13C and MS15A and their cellular correlation. **c** Enrichment analysis using gene ontology datasets. OPC = Oligodendrocyte progenitor cell, vSMC = Vascular smooth muscle cell, OLG = Oligodendrocyte, GO = Gene ontology

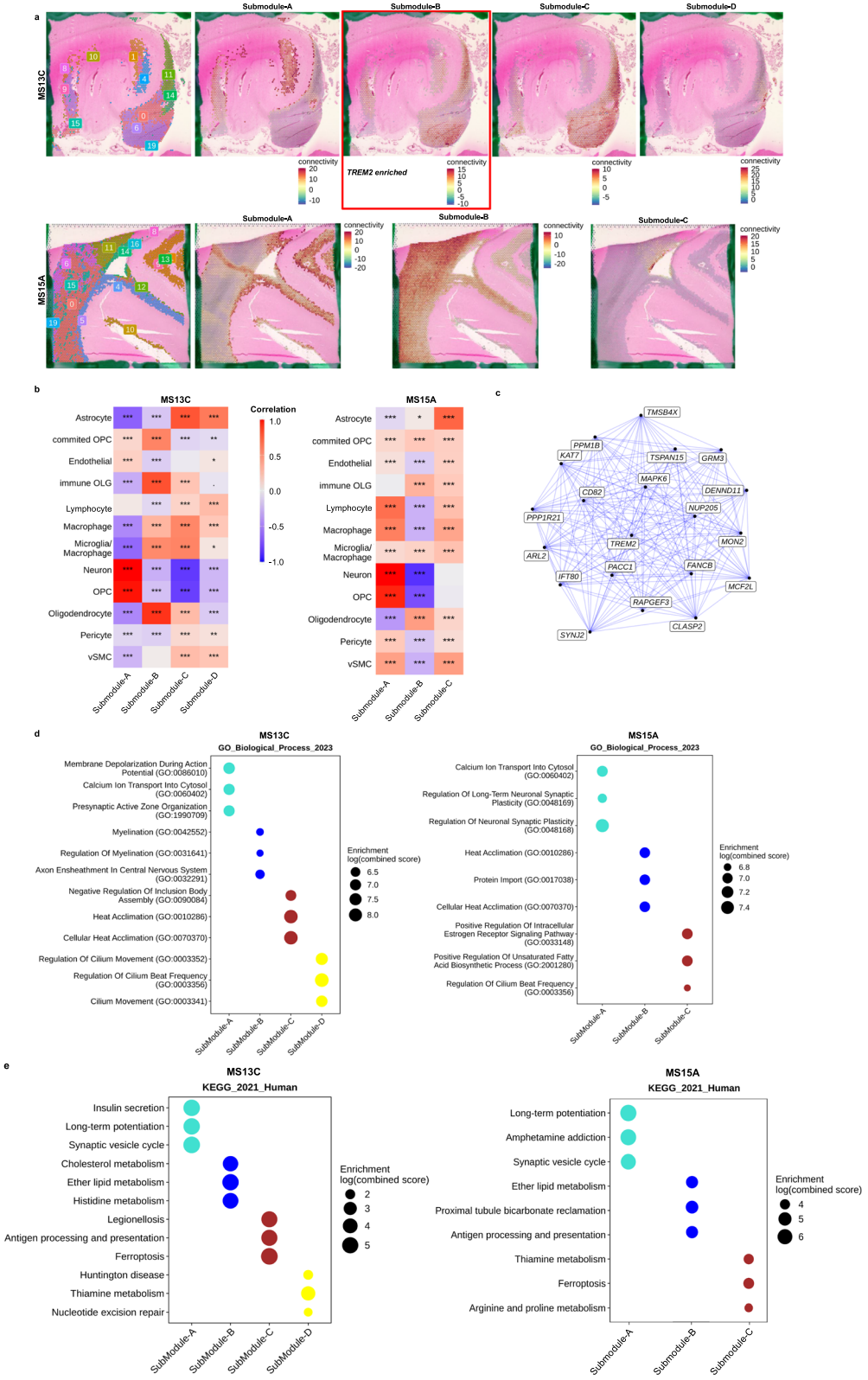

Fig. 3 (See legend on next page.)

(See figure on previous page.)

Fig. 3 Gene enrichment pathway analysis of module B revealed lesion-associated submodules, with TREM2 enriched exclusively in submodule B. **a** Submodules of original module B for the two cases MS13C and MS15A allowed the identification of submodules associated with distinct glial cell states. **b** Heat map of the cellular composition of each submodule for MS13C and MS15A. **c** Submodule B hub gene network for MS13C revealed *TREM2* and proximal genes. **d** Gene ontology biological process enrichment analysis for each submodule for MS15A and MS13C. **e** The results of enrichment analysis within the KEGG gene sets database for co-expressed glial submodules for MS13C and MS15A are shown. OPC = Oligodendrocyte progenitor cell, vSMC = Vascular smooth muscle cell, OLG = Oligodendrocyte, GO = Gene ontology

were abundant in microglia/macrophages and oligodendrocytes. Submodule B in MS13C contained expression of myelination pathway genes, reflecting the abundance of oligodendrocytes. Interestingly, submodule B of MS13C was the only submodule with *TREM2* expression enrichment (Fig. 3a and Fig. 3c). Network analysis of hub genes associated with *TREM2* from submodule B revealed functions relating to: cytoskeletal actin, tubulin motile and sensory cilia dynamics (*TMSB4X, MCF2L, ARL2, CLASP2, IFT80*); clathrin coated pits, endosomal maturation, vesicle trafficking and myelination (*PPP1R21, SYNJ2, MON2*); intracellular signalling relating to lipid metabolism, stress responses, oligodendrocyte migration and differentiation (*PPM1B, RAPGEF3, DENND11, MAPK6*); plasma membrane receptors, channels and signalling (*CD82, PACC1, GRM3, TSPAN15*); DNA repair, transcription and nucleocytoplasmic transport (*NUP205, FANCB, KAT7*). Further highlighting lipid metabolic pathways, additional enrichment analysis using the KEGG database revealed the cholesterol pathways involved within each submodule (Fig. 3e). Both cases were enriched in lipid metabolism genes in their submodule B (rim of MS13C and PLWM in MS15A) and ferroptosis genes in submodule C (lesion core and periphery). Submodule B of MS13C was enriched in cholesterol metabolism genes, essential for the breakdown of myelin [35]. The analysis also highlights the involvement of antigen processing and presentation pathway genes in the lesion core of MS13C (submodule C) and PLWM of MS15A (submodule B), which are involved in immune cell activation and cytokine production (Fig. 3e). Submodule D in MS13C was associated with vascular structures inside the lesion centre and meninges, and submodule C in MS15A, which lines the ventricle, showed enrichment in genes relating to pathways of cilium movement. These areas were rich in astrocytes, vascular smooth muscle cells, and lymphocytes (Fig. 3b).

TREM2 protein is low in microglia and PVMs in normal-appearing white matter from control or MS cases

To validate spatial transcriptomic results and better understand the types of CNS resident myeloid cells that express TREM2, its distribution was examined by immunofluorescence in MS and control tissues (Table 1). Myeloid cells in control CNS grey matter and NAWM are restricted to microglia and PVMs, which can be distinguished based on morphology, localisation and whether they express CD163. In control tissue, PVMs are half-moon-shaped CD163+ cells confined to the abluminal surface of vessels, whereas microglia are ramified Iba1+ cells (and more than 98% are negative for CD163), found throughout the parenchyma (Supplementary Fig. 2a–d). Microglia are further distinguished from PVMs by their extensive cytoplasmic processes and tiling of the parenchyma, not restricted to vessels. We measured a higher density of microglia (~ 100 cells/mm^2, see below), compared to CD163+ PVMs (~ 20 cells/mm^2; Supplementary Fig. 2c, d) in NAWM.

Triple immunofluorescent labelling of control tissues using Iba1, CD163, and TREM2 antibodies revealed most microglia and PVMs (> ~ 85%) in non-MS NAWM were TREM2-negative (Fig. 4 and Supplementary Fig. 2b). Limited data is available on TREM2 protein immunolabelling in human CNS tissues [36, 37]. We tested five commercially available TREM2 antibodies (Table 2), but some did not label microglia, PVMs or other macrophages in either healthy control or MS-lesioned human tissue. AF1828 and PA5-87,933 TREM2 antibodies intensely labelled endothelial cells in MS-lesioned and control tissue (Supplementary Fig. 2b). In our hands, AF1828, but not PA5-87933 TREM2 antibodies, reliably labelled myeloid cells (in addition to endothelium cross-reactivity). We used isotype control goat IgG as a negative control for AF1828 antibody immunofluorescence to confirm the positive labelling of microglia/PVMs. All subsequent work utilised AF1828 for TREM2 immunolabelling, which has also been previously reported to label microglia in diverse human CNS tissues [36].

TREM2 localisation in CD163+ lipid-laden PVMs, parenchymal macrophages and microglia in active MS lesions

MS tissues contain infiltrating myeloid cells, resident microglia, and PVMs that are reacting and proliferating. TREM2 immunolabelling was performed on 13 distinct active MS white matter lesions (with active centres) from 12 individuals (Fig. 4). The histopathology of these active lesions was characterised by the presence of ORO+ (lipid-filled) and CD68+/MHC class II+ reactive macrophages/microglia/PVMs that were localised to demyelinated lesion centres identified by pale LFB staining and reduced MBP immunohistochemistry compared to white matter adjacent to the lesion (PLWM) (Supplementary Fig. 3a). The ORO-stained, CD68+ cells were in the parenchyma

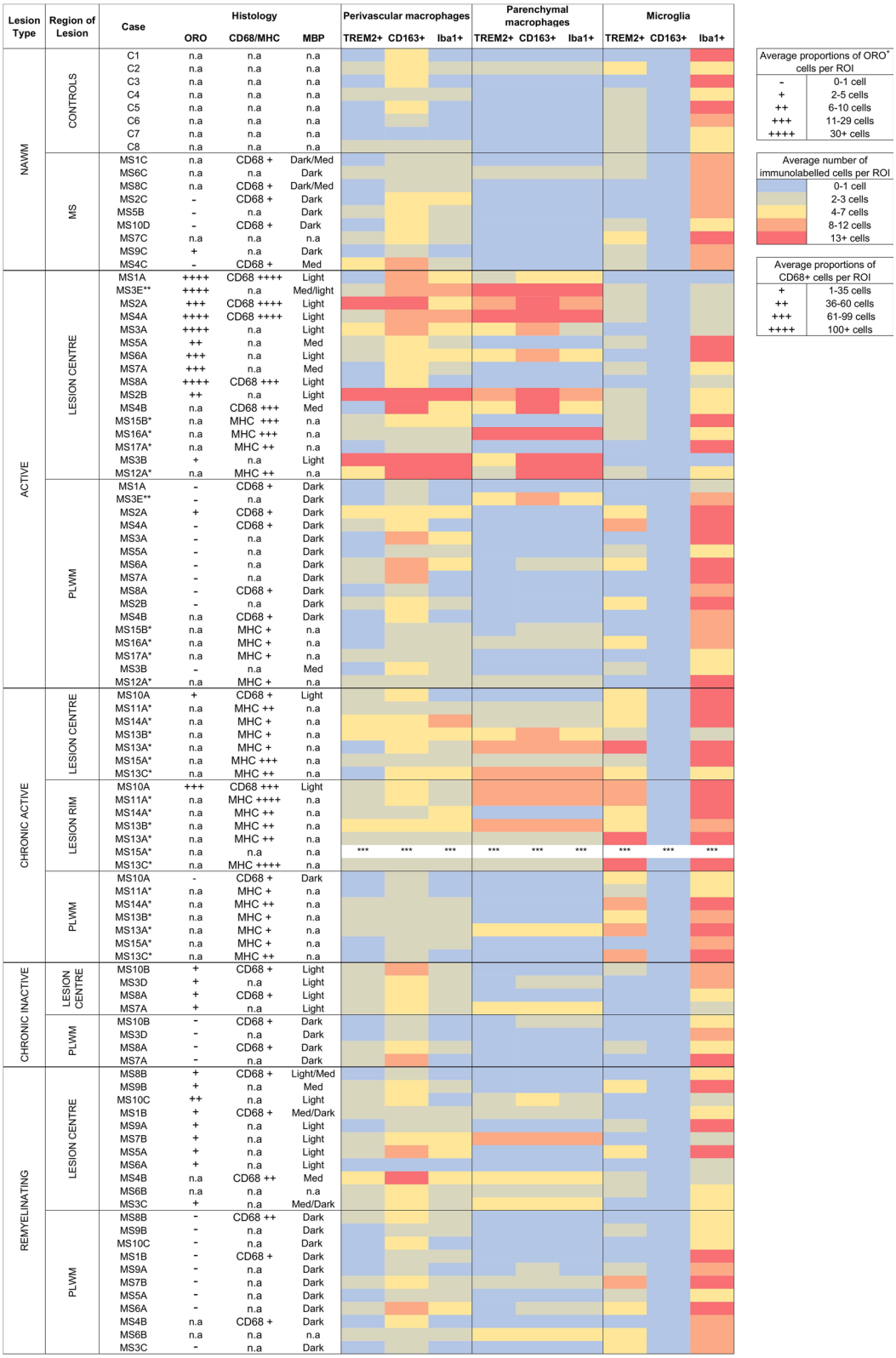

Fig. 4 (See legend on next page.)

(See figure on previous page.)

Fig. 4 Heat map highlighting heterogeneity of TREM2 protein expression in myeloid cells in MS lesions, MS and control NAWM. NAWM and lesion subareas were analysed (lesion centres, PLWM and lesion rims). Staining intensity for ORO, CD68+, MHC class II+ and, MBP+ for each tissue are shown. ORO+ cells per ROI (314.74 × 236.06 microns) ranged from 0 to 30 + cells. CD68+ or MHC class II+ cells per ROI (500 × 500 microns) ranged from 0 to 100+ cells. Relative MBP immunohistochemistry was characterised as "light", "med" and "dark". The three main cell types analysed were: PVMs (left), parenchymal macrophages (middle) and microglia (right). Images used to calculate the average number of immunolabeled cells per ROI were 312.39 × 312.39 µm. *Tissue lesions provided by Washington University Repository were identified by LFB and MHC class II staining. **MS3E was a case with active MS lesions, which subsequently was identified to have progressive multifocal leukoencephalopathy. This case was not included in subsequent overall analyses of the cohort of MS lesion cases. ***MS15A was a chronic active lesion confirmed by a neuropathologist, however the section provided did not have a clearly identifiable rim. ORO = Oil Red O, MBP = Myelin Basic Protein, NAWM = Normal-appearing white matter, PLWM = Perilesional white matter, n.a = not applicable, ROI = Region of Interest, MHC = MHC class II

as well as in contiguous rows on abluminal vessel surfaces in active demyelinating lesion centres (Fig. 5a). PVMs were also stained with LFB, indicating their cytosolic accumulation of myelin lipid and protein products (Fig. 5a). PLWM contained few or no ORO-stained cells (Supplementary Fig. 3a, b). By contrast, NAWM from unaffected areas of the CNS from 8 individuals with MS were characterised by the absence of ORO-stained PVMs and parenchymal cells (Supplementary Fig. 2a). PLWM and NAWM both had few CD68+ cells within the parenchyma (Supplementary Fig. 2a, Supplementary Fig. 3).

Triple immunofluorescent labelling using Iba1, CD163 and TREM2 antibodies revealed that active demyelinating MS lesion centres contained abundant CD163+ macrophages and CD163-negative hypertrophic microglia, which were both TREM2+ (Fig. 5b). In contrast to their isolated localisation to vessels and low density in NAWM (Supplementary Fig. 2b), CD163+ PVMs in active demyelinating lesion centres were grouped in contiguous rows along the abluminal surface of vessels and were often TREM2+ (Figs. 4 and 5b). These cells correlated with ORO+ PVMs stained in parallel sections of the same tissue blocks (Fig. 5a). TREM2 distribution differed between macrophages and microglia (Fig. 6a–f). Parenchymal macrophage infiltrating cells distal to vessels had a round soma without cytoplasmic processes and exhibited CD163, Iba1, and TREM2 immunolabeling at/near the plasma membrane. In contrast, microglia had smaller soma, contained cytoplasmic processes, were (mostly) negative for CD163, exhibited a more punctate appearance of the Iba1 immunolabelling distributed internally as well as peripherally, and contained TREM2 peri-nuclear labelling internally when present. Occasionally, CD163+ putative microglia were found in active MS tissue, and these could be TREM2+ or negative. In summary, active demyelinating MS lesion centres contain TREM2+ immunolabelling in three distinct populations of myeloid cells: (1) CD163+ PVMs, (2) CD163+ parenchymal macrophages and (3) reactive microglia (Figs. 4 and 5). In addition, immunofluorescent labelling of MS13C shows that choroid plexus-associated macrophages express CD163, Iba1 and TREM2 in MS, consistent with the spatial transcriptomic data (Fig. 5c).

Abundant TREM2+ reactive microglia in the rim of chronic active MS lesions

TREM2 labelling was evaluated in 6 chronic active white matter lesions from 4 individuals with MS (Table 1). Chronic active lesions were characterised histologically by the presence of CD68+/MHC class II+, ORO-stained microglia/macrophages in a peripheral rim of cells surrounding a demyelinated and comparatively hypocellular lesion centre (Supplementary Fig. 3b). Triple labelling of chronic active lesions with Iba1, CD163 and TREM2 antibodies revealed that, similar to active lesion centres described above, PVMs in chronic active lesion rims were also found in contiguous rows and were positive for CD163, Iba1 and TREM2 (Fig. 4). Whilst these lesions showed some heterogeneity in the distribution and density of myeloid cells, the chronic active rim was dominated by microglia (CD163-negative, Iba1+ TREM2+ cells with cytoplasmic processes) and CD163+ PVMs, with fewer macrophage infiltrates (rounded CD163+ cells), consistent with previous literature [38]. In summary, the most prominent parenchymal TREM2+ cell population in the chronic active rim were Iba1+ microglia, with a minority proportion of these microglia also positive for CD163.

Fewer TREM2+ microglia and macrophages in inactive and remyelinating MS lesions compared to actively demyelinating areas

TREM2 labelling was evaluated in 4 chronic inactive and 11 remyelinating MS lesions from 4 to 9 individuals, respectively (Table 1 and Fig. 4). Chronic inactive lesions were characterised by hypocellular, ORO-negative demyelinated centres with very few CD68+/MHC class II+ cells (Supplementary Fig. 4a). Remyelinating lesions were largely ORO-negative with patchy MBP labelling and CD68+/MHC class II+ cells concentrated in the perivascular areas (Supplementary Fig. 4b). Chronic inactive lesion centres mostly lacked CD163+ macrophages but contained Iba+ microglia. Remyelinating lesion areas were also dominated by Iba1+, CD163-negative microglia. In chronic inactive and remyelinating lesions, fewer microglia were TREM2+ compared to areas of active demyelination (Fig. 4).

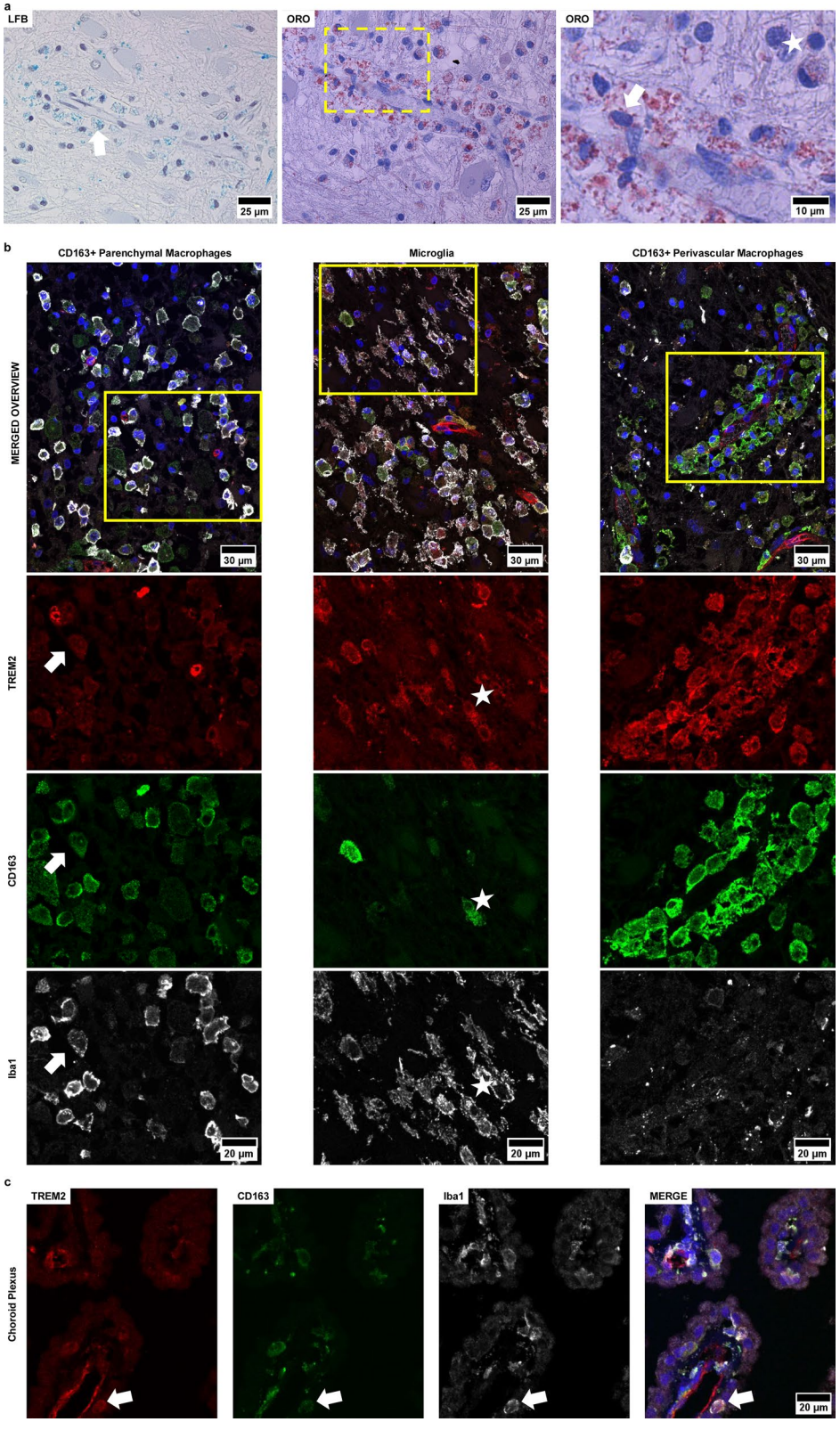

Fig. 5 (See legend on next page.)

(See figure on previous page.)

Fig. 5 Characterisation of TREM2 expression on microglia and macrophages in active lesions. **a** Representative Luxol Fast Blue (LFB) and Oil Red O (ORO) images from MS2A highlight the histopathology of an active MS lesion. Lipid-filled cells in the active lesion are highlighted by LFB staining (left; 25 µm scale bar) and ORO staining (middle; yellow dotted box highlights the area of the right image; 10 µm scale bar). Arrows point to LFB staining inside PVMs (possibly indicative of intracellular myelin products—white arrow), ORO + cells in the CNS parenchyma (white star) and lining the vessel (white arrow) (×40 magnification). **b** Representative immunofluorescence images of macrophages (left), reactive microglia (centre), and PVMs (right) are from active lesions (from MS2A and MS4A) (×40 magnification; 30 µm scale bar). Cropped images are from the highlighted area in the merged overview (yellow square). The area has been split into separate channels: TREM2 (red), CD163 (green) and Iba1 (white). DAPI-stained nuclei (blue) are only seen in the merged overview images. The white arrow marks a triple-labelled TREM2+ CD163+ Iba1+ macrophage. The star marks a rare putative triple-labelled TREM2+ CD163+ Iba1+ microglia. In this panel, other reactive microglia can be seen that are negative for CD163. **c** TREM2 (red), CD163 (green) and Iba1 (white) triple-labelled macrophages in the choroid plexus (white arrow) from MS15A (20 µm scale bar)

Quantification of regionally distinct profiles of TREM2+ microglia and macrophages in MS and control tissues

To quantify the number of TREM2+ cells across the different tissues analysed and described above, we evaluated white matter total cell density (DAPI-stained—all cells in the parenchyma region of interest), total microglia/macrophages (Iba1+ and/or CD163+), and the TREM2+ proportions of microglia/macrophages in the different MS and control tissues (Fig. 7a–d). As expected, there were significantly more microglia/macrophages in active lesion centres and chronic active lesion rims than in NAWM or PLWM (Fig. 7b). The overall density of Iba1+/CD163+ microglia/macrophages in PLWM was similar or slightly elevated compared to control and MS NAWM. The density of TREM2+ microglia/macrophages was significantly elevated in active lesion centres and chronic active lesion rims compared to NAWM (Fig. 7c, d). Remyelinating lesions contained significantly lower densities of microglia/macrophages compared to actively demyelinating areas (active centre and chronic active rim) and correspondingly fewer TREM2+ cells. However, these areas of remyelination did not completely resemble control NAWM with low densities of TREM2+ cells (Fig. 7c–e).

Quantification of the relative proportions of single-labelled (TREM2+ or Iba1+ or CD163+), double-labelled (any combination of two markers) or triple-labelled (TREM2+, Iba1+ and CD163+) cells in NAWM, active demyelinating, chronic active and remyelinating lesions, revealed distinctly different phenotypes of microglia and macrophages associated with the different types of MS lesional activity (Fig. 7e). The dominant cells in active lesion centres were triple-labelled Iba1+ CD163+ TREM2+ parenchymal macrophages (44%), with single-labelled Iba1+ microglia (19%). By contrast, in chronic active lesion rims, the dominant cell types were double-labelled Iba1+ TREM2+ microglia (44%) and single-labelled Iba1+ microglia (33%), with 19% of cells being triple-labelled Iba+ CD163+ TREM2+. This confirms that chronic active lesion rims contain more microglia (that are generally CD163-negative) than CD163+ macrophages. Interestingly, PLWM around both chronic active lesions and active lesions was also dominated by microglia, with single Iba1+ cells (47–51%) and double-labelled Iba1+ TREM2+ cells (38–43%) (There were less than 10% CD163+ cells in PLWM). The centres of remyelinating lesions were dominated by single Iba1+ labelled microglia (57%) but also contained double CD163+ TREM2+ (15%) and triple Iba1+ CD163+ TREM2+ (14%) labelled macrophages. Overall, these data further support the conclusion that TREM2 is expressed in both CD163+ macrophages that are most abundant in active demyelinating lesion centres, as well as in Iba1+ microglia that represent the most abundant cell type in chronic active lesion rims. TREM2+ microglia also variably comprise a prominent fraction of cells in the perilesional areas proximal to either active lesion centres or to rims of chronic active lesions (Fig. 7c, d). TREM2+ cells that were negative for both CD163 and Iba1 (Fig. 6f) represented < ~2% of all labelled cells in all tissues examined (Fig. 7e).

Immunofluorescence intensity was measured to further evaluate microglia/macrophage activation states in the tissues. To account for immunofluorescence variability inherent to individual tissue blocks/sections, we measured intensities per cell in 12 independent NAWM tissue sections (6 MS and 6 controls) imaged under the same conditions. We also measured immunofluorescence intensities on the same pieces of tissue, comparing demyelinating areas, perilesional areas and remyelinating tissues (n = 6 sections per lesion type). The changed reactive state of microglia in actively demyelinating and perilesional areas was suggested by the elevated relative intensity of Iba1+ immunofluorescence per cell in these areas compared to NAWM (Fig. 7f). The intensity of TREM2+ and CD163+ immunofluorescence per cell was also elevated in active demyelinating lesion centres compared to PLWM on the same sections of tissues (Fig. 7f). The Iba1+ and TREM2+ fluorescence intensities per cell were lower in remyelinating tissues compared to more actively demyelinating tissues but were still higher than in NAWM areas.

TREM2+ microglia and macrophages co-express markers of activation and lipid droplet storage

TREM2 is implicated in lipid storage and metabolism (evident in the spatial transcriptomic analysis), and we therefore conducted immunofluorescent labelling for phagocytic activity, lipid droplet metabolism and cell activation in different MS lesions. PLIN2 (a lipid

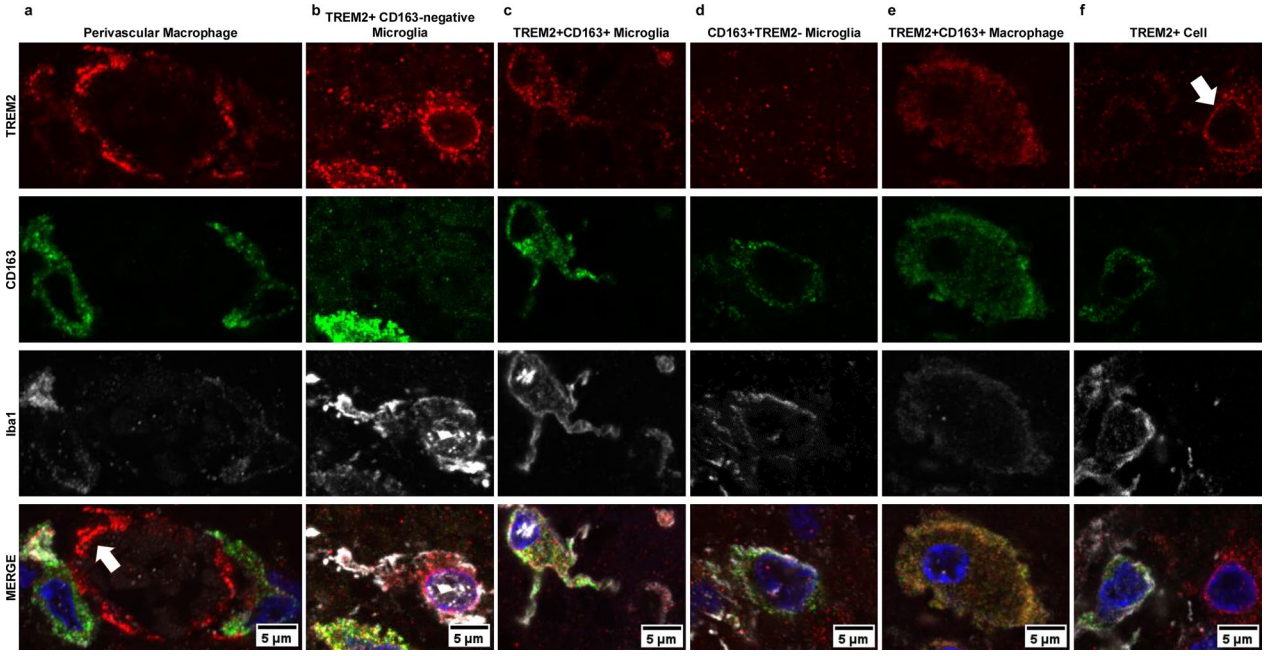

Fig. 6 Perinuclear and plasma membrane distribution of TREM2 respectively in microglia and macrophages in MS lesions. Actively demyelinating tissues were immunolabelled with TREM2 (red), CD163 (green), Iba1 (white), counter-stained with DAPI (blue; merged images), and imaged using a 100× objective with 6-step confocal z-stacks. **a** Triple labelled PVM–CD163+ TREM2+ Iba1+ (case MS4A). Punctuate discontinuous labelling with the AF1828 antibody in a thin line around the inner surface of the vessel can also be seen, indicative of endothelium (arrow). **b** TREM2+ CD163-negative microglia (MS2A), **c** TREM2+ CD163+ putative microglia (MS2A), **d** TREM2-negative CD163+ putative microglia (MS4A), **e** CD163+ TREM2+ macrophage (MS2A). **f** A rare TREM2+ CD163-negative Iba1-negative cell (white arrow) (MS4A). Scale bars = 5 µm

droplet coating protein) expression was most prominent in contiguous rows of PVMs in actively demyelinating areas, where many of these cells were also MHC class II+ (Fig. 8a), whilst in NAWM, PLIN2+ cells were rare or absent. The proportion of parenchymal cells positive for PLIN2 was significantly greater in active lesion centres (45% of cells) and chronic active rims (27% of cells) compared to perilesional areas (4% of cells) and NAWM (< 2.5% of cells) (Fig. 8b). Of the PLIN2+ cells, 7% were TREM2+ in the active lesion centres, whereas 14% were TREM2+ in the chronic active rim and 12–17% were TREM2+ in perilesional areas. TREM2+ PLIN2+ double-labelled cells were not detected in NAWM. Notably, PLIN2+ cells were far more abundant than TREM2+ cells in actively demyelinating areas; however, the vast majority of TREM2+ cells also expressed PLIN2, highlighting an overlap between these cell populations. We further investigated TREM2 co-expression with MHC class II, CD68, and TMEM119 (Fig. 8a and c and Supplementary Fig. 5a–d). As expected, in active lesions, there were significantly more MHC class II+ cells (43% of cells) than in perilesional areas (12% of cells). Prominent MHC class II labelling was on both parenchymal macrophages/microglia and PVMs (Fig. 8a). Of the MHC class II+ cells, 33% of them in the lesion and 12% in the peri-lesional area were TREM2+ (Supplementary Fig. 5a). The percentage of CD68+ cells in active lesion centres was 37%, compared to 8% in the PLWM. Of the CD68+ cells, 10–15% were positive for TREM2 in both lesion centres and perilesional areas (Fig. 8c and Supplementary Fig. 5b). There was no difference in the percentage of TMEM119+ cells in active lesion centres compared to perilesional areas (~ 10–25% of all cells). Of the TMEM119+ cells, ~ 25% were TREM2+ in active lesion centres and ~ 10% in the peri-lesion area (Supplementary Fig. 5c).

MS4A4A is highly expressed on CD163+ TREM2+ parenchymal and perivascular lipid-laden macrophages in a case of progressive multifocal leukoencephalopathy

Patient MS3 (41-year-old male) had SPMS, and post-mortem analysis led to an added diagnosis of progressive multifocal leukoencephalopathy (PML), positive for JC virus. This case was excluded from all of the above analyses of TREM2 expression in MS. ORO stained an extensive area of tissue in the MS3E block (Fig. 9a), corresponding to abundant macrophages with CD163+ and TREM2+ labelling localised to/near the plasma membrane (Fig. 9b). Immunolabelling with microglia marker TMEM119 was negative in this area (Fig. 9c), while MS4A4A labelling was prominent (Fig. 9d). MS4A4A is a cell surface macrophage-regulating protein with genetic linkage to CSF levels of the soluble form of TREM2 [19]. The abundant CD163+ Iba1+ cells in the PML lesion that co-labelled for MS4A4A were TMEM119-negative

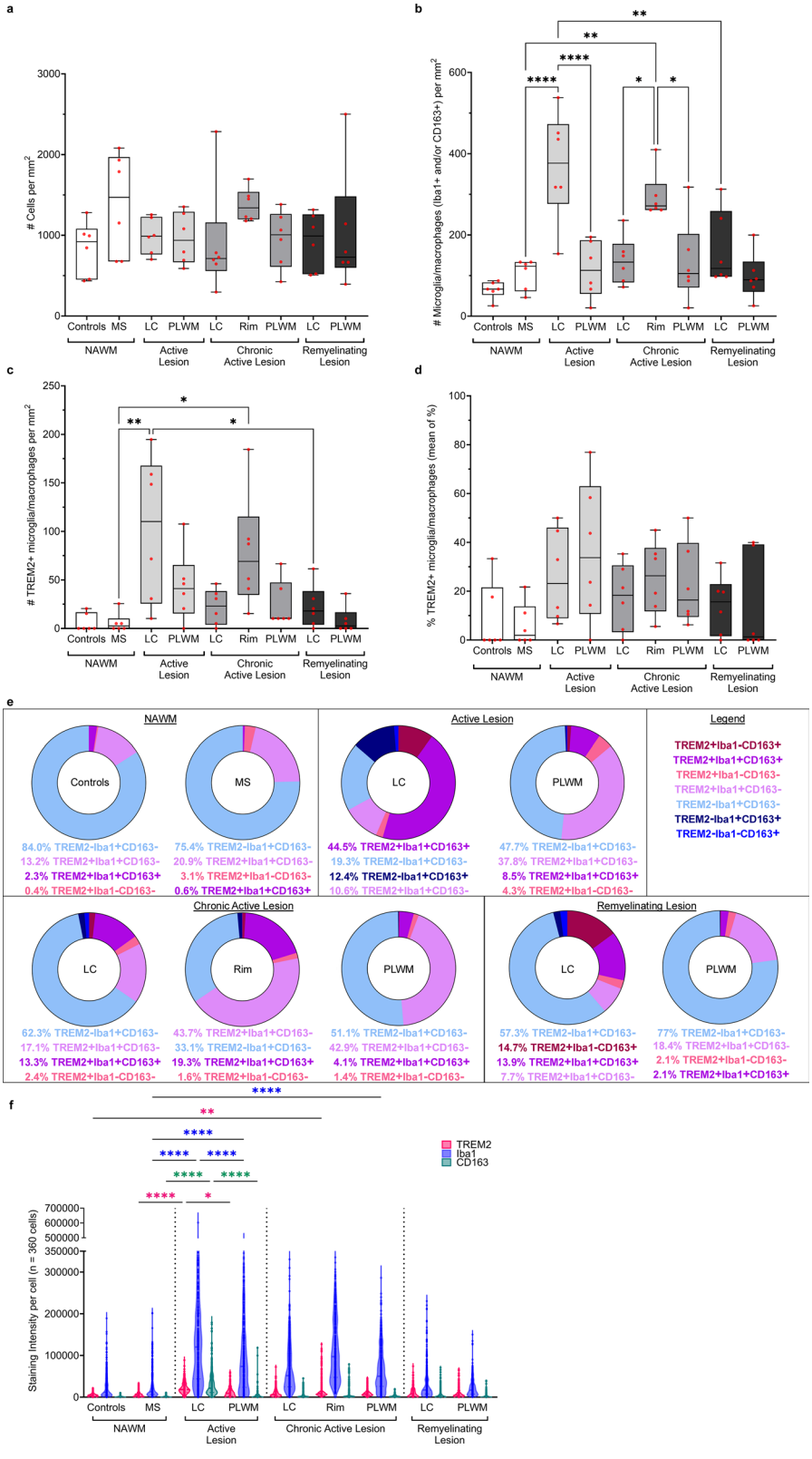

Fig. 7 (See legend on next page.)

(See figure on previous page.)

Fig. 7 Quantification of TREM2+ cells in control NAWM, MS NAWM and MS lesions. **a** Number of cells (total DAPI nuclei) per mm^2, **b** number of microglia/macrophages (Iba1+ and/or CD163+) per mm^2, **c** number of TREM2+ microglia/macrophages per mm^2, and **d** percentage of TREM2+ microglia/macrophages in distinct tissue areas as indicated. **e** Proportions of single, double, and triple labelled TREM2+ CD163+ Iba1+ cell populations in distinct tissue areas. The four most abundant cell phenotypes for each area are listed below each chart. Each cell phenotype has been referenced with the same colour across different lesion types as indicate in figure legend. **f** Immunofluorescence intensity of TREM2 (pink), Iba1 (blue) and CD163 (green) in distinct tissue areas. The size of the individual cell region of interest used to determine intensity ranged from 64 to 295 μm^2. *$P \leq 0.05$; **$P \leq 0.01$; ****$P \leq 0.0001$. NAWM = normal-appearing white matter (from MS cases or controls as indicated), LC = lesion centre, PLWM = perilesional white matter, LR = lesion rim

(Fig. 9c, d), further suggesting that this TREM2+ CD163+ MS4A4A+ cell population is dominated by macrophages and not microglia. In the perilesional area, TREM2+ TMEM119+ CD163-negative microglia were observed in this case (Fig. 9e). MS4A4A labelling was weaker and less striking in pure MS tissues compared to the PML case. In MS lesions, MS4A4A+ cells were more often found in the active lesion centre (27% of cells) compared to the perilesional areas (7% of cells), with 44% of MS4A4A+ cells also TREM2+ in the centre and 23% in the perilesional area (Supplementary Fig. 5d). MS4A4A labelling was most prevalent on PVMs (Fig. 9f) and parenchymal macrophages but was also seen on some microglia.

Discussion

Reactive microglia and macrophages are characteristic immune cells of demyelinating MS lesions [39]. Depending on their functional state, they can contribute both to lesion resolution or progression in ways not yet fully understood. Here, we reveal bespoke properties of different myeloid cell populations in MS white matter lesions and PLWM compared to NAWM from MS and non-neurological disease control cases. This work contributes towards understanding the distinct spatial patterns of gene and protein expression related to the dynamic functions of myeloid cells in MS lesions across the disease trajectory, which could inform future strategies to harness the reparative functions of myeloid cells while inhibiting those that drive disease progression.

Spatial transcriptomics analysis showed conserved cellular and molecular compositions of MS tissues despite histopathological differences. This suggests that lesion pathology is influenced not only by the presence of specific cell types, but also by their spatial organisation and activation states. We focused on TREM2 because this innate immune cell receptor has been found to exert protective functions in preclinical models of demyelination/remyelination relevant to MS [10–13, 39, 40]. TREM2 deficiency results in altered lipid homeostasis, impaired intracellular lipid droplet metabolism and reduced myelin clearance in microglia, which could delay remyelination in the context of MS [10, 17, 39]. Further, TREM2 is a candidate participant, more generally, where response to demyelination and repair is needed—for example, relating to Alzheimer's disease pathology, where there is aging-associated loss of myelin integrity and neuroinflammation [41–43]. Of note, in this context, TREM2 genetic variants are a risk factor for Alzheimer's disease [44, 45]. We verified that TREM2 is expressed in actively demyelinating MS white matter and PLWM areas across diverse brain regions in different people with MS, and we detected far fewer TREM2+ cells and weaker immunofluorescence intensity in NAWM of MS and non-neurological disease controls. Spatial transcriptomics in two MS hippocampal tissues revealed myeloid cells expressing *TREM2* with different spatial organisation relative to pathological features. For example, relating to the chronic active lesion, *TREM2*+ cells co-expressing *CD68* were prominent in the lesion centre and *TREM2*+ *CD163*+ cells in rim areas. This suggests heterogenous gradients of different gene expression in TREM2+ cells depending on their localisation. *TREM2* was largely restricted to areas enriched in glial cells expressing genes encoding lipid and cholesterol metabolic pathways, which mostly corresponded spatially to the white matter chronic active lesion rim. This is consistent with previous reports revealing unique transcriptional properties of the chronic active rim, including expression of iron and lipoprotein metabolism genes, which correlate with disease progression [46, 47]. Our transcriptomic analysis further showed that tissue areas corresponding to the chronic active lesion centre and perilesional areas were enriched in expression of gene pathways related to ferroptosis, cellular heat acclimation, and myelination, which could indicate the presence of attempted reparative functions in these areas. Evidence suggests that TREM2 expression in mouse and in vitro models is increased by induction of cellular heat acclimation pathways, and this may be a neuroprotective response in MS tissue [48, 49].

Application of co-expression network analysis (WCGNA) on *TREM2*+ tissue regions expands understanding of MS-related changes. This approach revealed a specific glial cell submodule B, enriched in the expression of genes involved in lipid and cholesterol metabolism, that is localised to the chronic active MS lesion rim and PLWM. *TREM2* expression was enriched exclusively in this submodule compared to other glial cell submodules spatially distal from active demyelinating or perilesional areas. Many of the submodule B enriched hub genes, align with recently published MS spatial transcriptomics data, highlighting consistent and relevant key functionalities upregulated in MS chronic active lesion rims and PLWM [40–42]. Hub gene *PPM1B* is involved in energy metabolism via the modulation of

fatty acid metabolism in lipid-laden foamy macrophages. This phosphatase also plays roles in signalling that negatively regulates TGFβ [43], which indicates anti-inflammatory pathways are active in submodule B. *CD82* is a tetraspanin family gene expressed in late lineage oligodendrocytes involved in differentiation and myelination and also in restricting oligodendrocyte precursor cell (OPC) migration [44]. The expression of this gene in submodule B suggests inhibition of OPCs is occurring, consistent with the lower abundance of these cells reported in areas of active demyelination [41]. Relating to this, hub gene *MAPK6* is involved in MAPK-ERK signalling in proliferating OPCs and inhibits their ultimate differentiation into mature remyelination-competent oligodendrocytes [45], suggesting OPC differentiation as well as migration could be negatively impacted in active lesion rims. Whilst cholesterol metabolism and cellular heat acclimation pathways linked to *TREM2* represent key steps towards tissue repair by setting the stage for remyelination, it is ultimately differentiation of myelination-competent oligodendrocytes that is required for full recovery and this step in the process of repair is potentially blocked in the milieu of chronic active MS lesioned tissue, for example by sustained activation of MAPK-ERK signalling [45]. In the context of myelination competency, our identification of a cilium movement-associated cell module in the lesion centre and lesion rim in demyelinating MS tissues is interesting, as recent findings suggest that OPCs require the construction of primary cilia for remyelination capacity [46]. MS13C submodule B hub gene *IFT80* encodes a protein involved in the assembly of motile and sensory cilia, which can be expressed in multiple cell types, including microglia and oligodendrocytes in the CNS. Previous studies have demonstrated that cilium-mediated activation plays a role in remyelination in MS [47]. Genes involved in control of cilia motility functions were also noted in previous spatial transcriptomics data sets, enriched in the inactive lesion centres where they were suggested to represent populations of ciliated astrocytes in the glial scar [41]. Of note, hub genes *TMSB4X* (encodes an actin-binding protein involved in cell motility, migration and immune invasion), *PPP1R21* (encodes a protein phosphatase regulatory subunit implicated in myelination), and *TREM2* were all previously identified as enriched in chronic active lesion rims by spatial transcriptomics [40], consistent with our data. We further identified genes relating to endosomal function at the chronic active lesion rim, which is also consistent with previous work [41].

Immunofluorescence analysis enabled verification and further characterisation of TREM2 expression in MS tissues using a larger cohort of cases. We found that TREM2 is represented in heterogeneous populations of CD163-negative reactive microglia, CD163+ infiltrating parenchymal macrophages and CD163+ PVMs. The involvement of both reactive resident microglia as well as infiltrating macrophages has been previously described in MS [39], and we extend these studies to characterise TREM2 distribution in these resident and invading myeloid cell populations. Note that small numbers of dendritic cells (DCs) are present to a variable extent in MS tissues, particularly around small-calibre vessels, and we cannot discount that a small proportion of the perivascular TREM2+ cells that we observed may represent DCs [48].The variations in abundances of the different types of TREM2+ cells in distinct tissue areas further provide clues to their roles in the stages of lesion development, which may reflect MS disease trajectory. Firstly, unlike NAWM, PLWM contained significant TREM2+ microglial populations that had similarities to TREM2+ CD163-negative microglial cells at chronic active demyelinating white matter lesion rims. This is relevant because it shows that reactive TREM2+ microglia in the PLWM around both active and chronic active MS lesions, recapitulate some properties of microglia in chronic active lesion rims, distinct from homeostatic microglia in NAWM. These data align with evidence showing that NAWM and PLWM are transcriptionally distinct, and that *TREM2* transcripts are elevated in demyelinating chronic active lesion rims [40]. Secondly, in addition to microglia, we found that TREM2 is expressed in CD163+ infiltrating macrophages, which are abundant in the centre of active MS lesions. In NAWM of MS and controls, CD163+ cells corresponded almost entirely to resident border PVMs, which were restricted to abluminal vessel surfaces as lone isolated cells (fewer than 2% of microglia were CD163+), consistent with previous reports [7, 49]. This is different from actively demyelinating MS tissues, where we found contiguous rows of CD163+ cells along vessels, which may represent proliferating border PVMs that eventually infiltrate the parenchyma, or macrophages infiltrating through the vessel wall from the periphery: distinguishing between these two possibilities in human tissues is difficult [38, 50]. However, together with oligodendrocyte and OPC loss, these CD163+ macrophage infiltrates signify acute demyelination and inflammation [51–54]. Our data provide evidence that TREM2 expression on CD163+ infiltrates is likely a functional response to demyelination/tissue injury. CD163+ parenchymal macrophages were found in all areas where there was active demyelination (active lesion centres and rims of chronic active lesions), but were absent in PLWM, inactive lesions, and in NAWM. Overall, our data show that the majority of CD163+ cells associated with demyelination in active lesion centres were distinguished by a rounded morphology typical of peripheral macrophages with CD163+ and TREM2+ immunolabeling localised to the plasma membrane (different from the

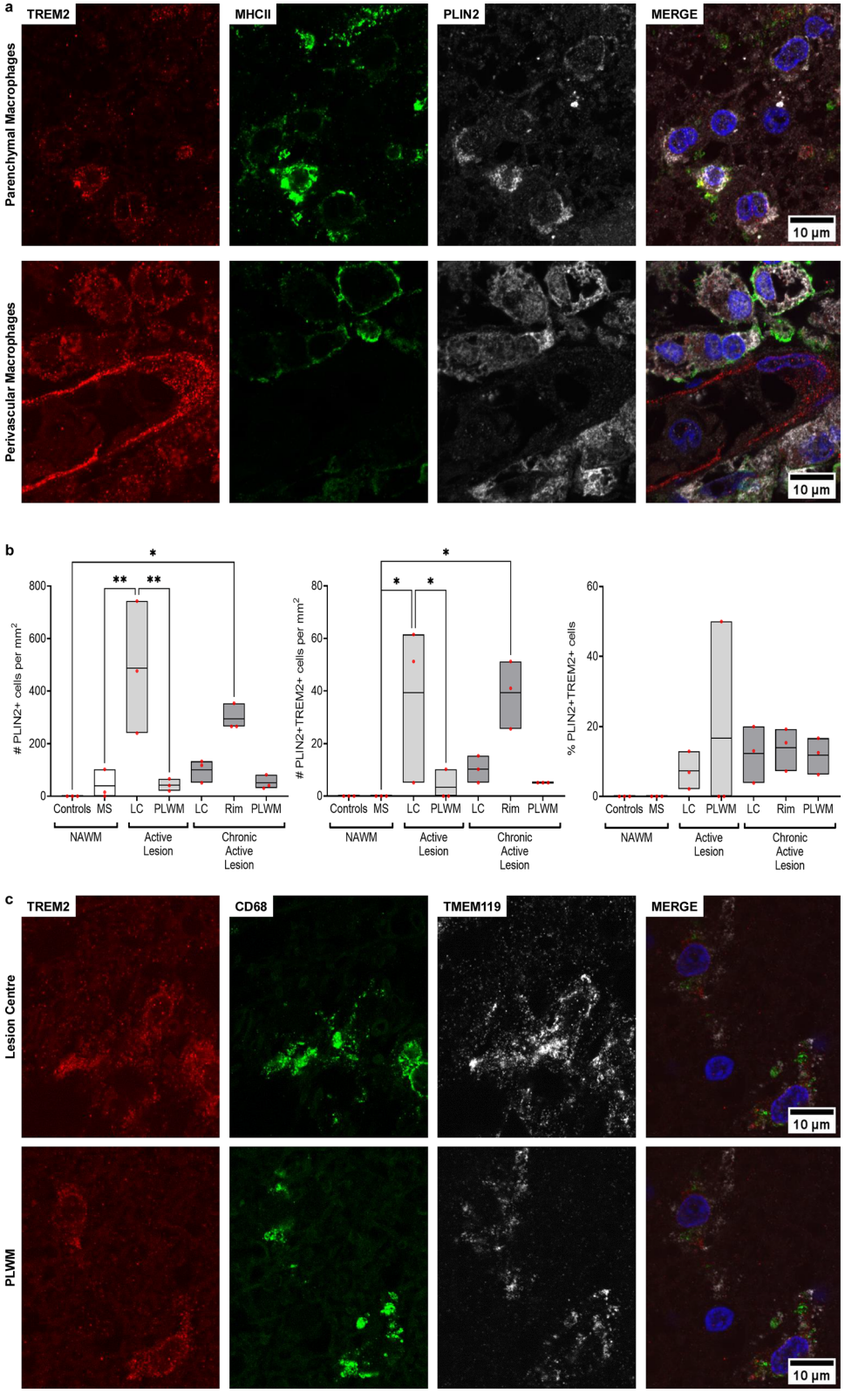

Fig. 8 (See legend on next page.)

(See figure on previous page.)

Fig. 8 TREM2 co-expression with lipid metabolism and activation markers. **a** TREM2 (red), MHC class II (green), and PLIN2 (white) immunolabelling in parenchymal macrophages (top) and perivascular macrophages (bottom) from an active lesion centre (MS2A). **b** Quantification per mm^2 of number of PLIN2+ cells, PLIN2+ TREM2+ cells and the proportion of all PLIN2+ cells that are TREM2+ in different tissue areas. All TREM2+ cells were PLIN2+. **c** TREM2 (red), CD68 (green) and TMEM119 (white) indicate TREM2 expression in active microglia in the lesion centre (top) and PLWM (bottom). DAPI nuclei counterstain is shown in the merged channels (100× objective; 10 µm scale bar) (MS4A). NAWM = Normal-appearing white matter, LC = lesion centre, PLWM = Perilesional white matter, LR = lesion rim

hypertrophic ramified shapes of typical reactive microglia, with perinuclear TREM2 labelling). Interestingly, CD163+ cells represented more than 50% of all myeloid cells in active lesion centres. By contrast, 19% of cells in chronic active lesion rims were CD163+ (and < 10% in PLWM). In chronic active lesion rims, TREM2+ CD163-negative microglia, as described above, were the most dominant reactive myeloid cells (44%). Previous work also reports that chronic active lesion rims are enriched in higher proportions of reactive microglia compared to infiltrating macrophages [1, 9, 38]. Our work extends these findings by demonstrating that TREM2 is prevalent in reactive rim microglia, where the co-expression of lipid and cholesterol metabolism genes dominates in and/or near these cells. The variation in proportions of macrophages and microglia in acute lesion centres compared to chronic active lesion rims and PLWM highlights the differing roles of myeloid cells in these distinct tissue areas, which likely represent different stages of the pathological demyelinating cascade. Lipid and cholesterol uptake, storage and efflux are essential for repair after demyelination, and these processes most likely reflect the abundance of TREM2+ microglia and macrophages in demyelinating tissues. However, if the system is overwhelmed by ongoing demyelination, these same cells may then represent markers of lesion progression. It remains to be established whether TREM2+ reactive microglia in PLWM and lesion rims represent cells that have undergone adaptation to respond protectively to demyelinating events and/or whether they represent cells that have transformed into primary drivers of lesion progression [40, 55].

Relevant to lipid metabolism associated with demyelination, intracellular lipid droplets (LD) are storage organelles involved in maintaining lipid homeostasis and preventing lipotoxicity [16, 56]. Prolonged accumulation of LDs in microglia can result in reduced phagocytic ability, the generation of reactive oxygen species and cascading inflammation [57]. PLIN2 is the most abundant CNS lipid droplet-coating protein, and we found that while all TREM2+ myeloid cells in actively demyelinating tissue areas were PLIN2+ , many PLIN2+ cells were negative for TREM2 or other myeloid cell markers. This indicates that lipid metabolism and storage in MS white matter involves other glial cell types in addition to TREM2+ myeloid cells [18, 58, 59].We established that PLIN2 was expressed in actively demyelinating lesion areas, was almost negligible in NAWM, and was found in relatively low abundance in PLWM. Significantly more PLIN2 was detected using immunofluorescence compared to transcriptomics, where lower transcriptomic detection can result from inadequate tagging or low yield, leading to undetected transcripts using Visium. A further limitation of Visium spatial transcriptomics used here, despite deconvolution, is the inability to spatially map single-cell data, where each spot contains approximately 1–10 cells. Nevertheless, PLIN2 transcripts were detected by spatial transcriptomics exclusively in clusters aligned with demyelinating lesion areas, albeit at low levels, and were not detected in non-lesional tissue areas. Using immunofluorescence in a larger cohort of cases, we found that abundant PLIN2+ myeloid cells were CD163+ (infiltrating parenchymal macrophages or PVMs). These PLIN2+ PVMs/macrophages were found in contiguous rows along the abluminal surface of vessels, supporting a prominent role for vessel-associated myeloid cells in lipid clearance and storage in MS [60].

One brain donor in our cohort was excluded from image analysis and myeloid cell quantification analysis as an MS case, because we discovered that this person with MS had treatment-induced PML. We observed abundant TREM2+ CD163+ parenchymal macrophage infiltrates in the tissues from this case, linking TREM2 expression with acute myeloid cell infiltrates that accumulate (ORO+ staining) lipids, and localise to areas of rapidly progressing demyelination. Notably, this case was the only one in our cohort that also showed substantial MS4A4A immunoreactivity. We were interested in MS4A4A because of its proposed role in pathways linked to TREM2 function [19, 22, 61]. We observed variable MS4A4A expression on some CD163+ macrophages and less so on microglia in active MS lesions, consistent with reports showing MS4A4A expression is associated with hematopoietic monocyte to macrophage differentiation [20]. By contrast, we found that most MS4A4A+ cells were negative for microglial marker TMEM119, suggesting MS4A4A may only be weakly expressed in resident CNS microglia. MS4A4A is reported to promote macrophage polarisation towards “anti-inflammatory” phenotypes [21, 62] and regulate the shedding of soluble TREM2 from the cell surface [19], thereby altering macrophage/microglial functions [63]. The presence of large numbers of MS4A4A+ TREM2+ CD163+ macrophages in the PML case and, to a lesser extent, in active MS lesions highlights

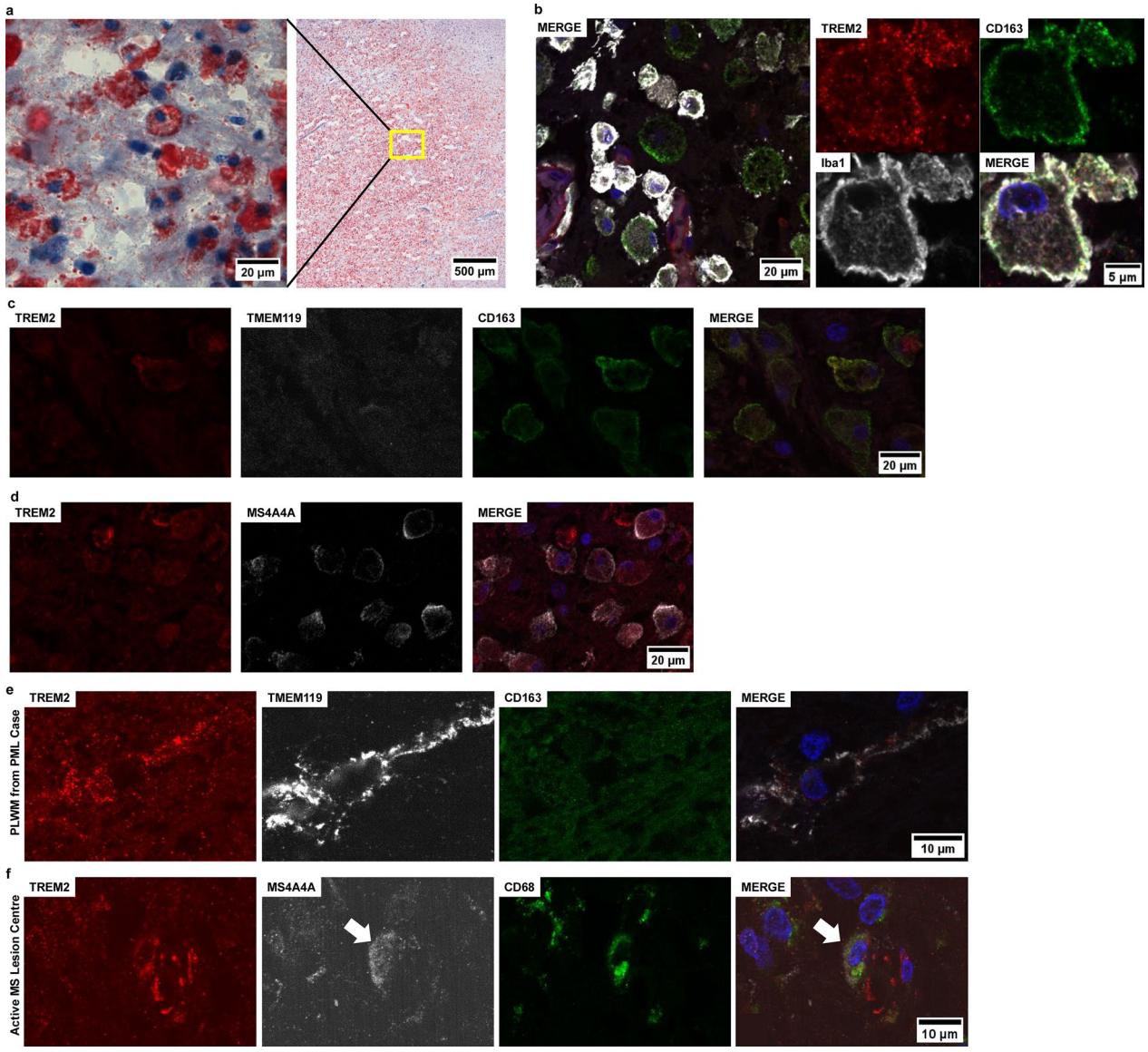

Fig. 9 TREM2 and MS4A4A expression in a PML and active MS lesion. **a** ORO staining of a PML lesion (20× objective; 200 µm scale bar). The insert (left) shows lipid-filled round macrophage infiltrates characteristic of PML (40× objective; 20 µm scale bar). **b** TREM2 (red), CD163 (green) and Iba1 (white) immunofluorescence with DAPI nuclei counterstain (blue), highlights abundant CD163+ TREM2+ Iba1+ triple labelled macrophages in the PML lesion with TREM2 distributed to the plasma membrane of foamy macrophages (merge panel 30 µm scale bar; right panels 5 µm scale bar). **c** TREM2 (red), TMEM119 (white), CD163 (green) and DAPI (blue), 20 µm scale bar. **d** TREM2 (red), MS4A4A (white) and DAPI (blue), 20 µm scale bar. **e** TREM2 (red), TMEM119 (white), CD163 (green) and DAPI (blue; merged image) indicate TREM2+ microglia in peri-lesional white matter in PML (10 µm scale bar). **f** TREM2 (red), CD68 (green) and MS4A4A (white) indicate TREM2 and MS4A4A co-expression in PVMs from an active MS lesion centre (MS4A). DAPI nuclei counterstain is shown in the merged channels (100× objective; 10 µm scale bar). Representative images in a–e are of tissue from PML case MS3E. PLWM = Perilesional white matter, PML = Progressive multifocal leukoencephalopathy

the interplay between TREM2 and MS4A4A functions in the context of acute demyelination, which merits further investigation [63].

In summary, this work highlights the expression of TREM2 in CD163+ macrophages associated with active demyelination, as well as in reactive microglia that dominate smouldering chronic active white matter rim lesions associated with disease progression. The similarities between the cellular composition of PLWM and chronic active lesion rims, including expression of TREM2, distinct from NAWM, is of importance, as it suggests that the PLWM may be involved in lesion expansion and progression. Finally, abluminal TREM2+ vessel macrophages appear to play an important role in lipid metabolism and storage in the context of active demyelination. The functional involvement of TREM2 in MS lesion progression requires further investigation to determine the extent of its impact on myelin turnover, lipid phagocytosis, storage

and detoxification, but also its potential relationship to toxic macrophage/microglia phenotypes that might adapt to drive disease progression in MS.

Supplementary Information

The online version contains supplementary material available at https://doi.org/10.1186/s40478-026-02241-x.

Supplementary Fig. 1 Spatial distribution of *PLIN2* and *TMEM119* in glial submodules in MS13C and MS15A. Quantitative analysis of *PLIN2* and *TMEM119* myeloid cell markers in *TREM2* positive spots for MS13C (left) and MS15A (right). Supplementary Fig. 2 Perivascular macrophages in NAWM from controls and people with MS. **a** ORO, LFB staining and MBP and CD68 immunohistochemistry illustrate intact myelin, few reactive cells and no lipid-filled macrophages in NAWM (MS10D) (×40 magnification; 50 µm scale bar). **b** TREM2 (red), CD163 (green) and Iba1 (white) immunofluorescence with DAPI counterstain (blue; merged image) of control NAWM (top row; C1) and MS-NAWM (middle and bottom rows; MS7C and MS10D respectively). CD163+ PVMs (star) are illustrated in MS-NAWM (bottom row), where the AF1828 TREM2 antibody also labels endothelium (red) (white arrows) (20 µm scale bar). **c** The number per mm2 of CD163+ microglia (left) and percentage of total microglia (middle) in control and MS NAWM is shown. **d** The number of CD163+ PVMs per mm2 in control and MS NAWM. ORO = Oil Red O, LFB = Luxol Fast Blue, MBP = Myelin Basic Protein, MS = Multiple Sclerosis, ns = Not significant. Supplementary Fig. 3 Representative histological images of active and chronic active lesions. **a** Overview image shows the lesion centre and the PLWM from case MS2A (500 µm scale bar). The right panels show ORO and LFB staining and CD68 and MBP immunohistochemistry from the lesion centre (top) and the PLWM (bottom). **b** Overview image shows the lesion centre, rim and PLWM of a chronic active lesion (MS10A; 200 µm scale bar). Right panels show ORO, and LFB staining and CD68 and MBP immunohistochemistry from the lesion centre (top), lesion rim (middle) and PLWM (bottom). Other images, 30 µm scale bar. ORO = Oil Red O, LFB = Luxol Fast Blue, MBP = Myelin Basic Protein, PLWM = Perilesional white matter. Supplementary Fig. 4 Representative histological images and TREM2 immunofluorescence in chronic inactive and remyelinating MS lesions. **a** Chronic inactive immunohistochemistry staining with ORO, MBP and LFB (with CD68 counterstain), and immunofluorescence labelling with TREM2 (red), CD163 (green) and Iba1 (white) and DAPI nuclei counterstain (blue). **b** ORO, MBP and LFB immunohistochemistry of a remyelinating lesion and immunofluorescence labelling with TREM2 (red), CD163 (green) and Iba1 (white) and DAPI nuclei counterstain (blue). Immunohistochemistry scale bar = 200 µm, immunofluorescence scale bar = 20 µm. Representative histology images are from MS10B and MS5A for the chronic inactive and remyelinating lesions, respectively. Representative fluorescence images are from MS7A (chronic inactive) and MS4B (remyelinating). ORO = Oil Red O, MBP = Myelin Basic Protein, PLWM = Perilesional white matter. Supplementary Fig. 5 Proportion of TREM2+ cells expressing MHC class II, CD68, TMEM119 and MS4A4A in active MS lesions. Quantification of the percentage of cells expressing **a** MHC class II, **b** CD68, **c** TMEM119 and **d** MS4A4A in the active lesion centre and PLWM. The graphs also depict the proportion of TREM2+ cells for each marker. PLWM = Perilesional white matter.

Supplementary info/Link to spatial transcriptomic data The spatial Visium count matrices and processed data generated for this study are uploaded to the Synapse portal and can be accessed online through Synapse ID [syn69902953] (https://www.synapse.org/Synapse:syn69902953). The sequencing data is available for general research use with controlled access. Requests to access the sequencing data should be directed to the corresponding authors.Custom preprocessing and downstream analysis scripts required to reproduce the manuscript results are available at the Zenodo portal: https://zenodo.org/records/17184169

Acknowledgements
This study was made possible by the generous tissue donations of our donors and their families. We thank the MS Australia Brain Bank for providing MS tissues, the Sydney Brain Bank and NSW Brain Tissue Resource Centre for providing control tissues. We would like to extend a special thanks to Prof. Anne H Cross for providing some of the MS and control tissues included in this work (part of the Neuroinflammatory Disease Tissue Repository at Washington University, St. Louis) and for the critical review of the manuscript and to Assoc. Prof. Roberta Magliozzi for her assistance with characterization of the tissues used for spatial transcriptomic and with the critical review of the manuscript. We thank Sydney Microscopy and Microanalysis (Microscopy Australia) for access to equipment and expertise, especially microscopists Dr. Neftali Flores Rodriguez and Dr. Yingying Su and the Alafi Neuroimaging Laboratory at Washington University in St. Louis.

Author contributions
YAC, EA, LRW, OH, CG and LP designed the study. YAC, CG and WB performed immunofluorescence staining, image acquisition and data acquisition. LRW assisted in optimising the image analysis methods. EA and OH performed spatial transcriptomic preparation and analysis of sections. BB, DD, AA and MB assisted with histological analyses of human MS and control tissues. YAC, EA, WB, OH, LP and CG contributed to the interpretation of data. CG supervised the immunofluorescence portion of the study, and OH supervised the spatial transcriptomics. YAC, CG, EA, OH and LP contributed to the original draft of the manuscript and the preparation of the figures. All authors reviewed the manuscript and approved its contents before submission.

Funding
This work was supported by grants from MS Australia Research Grant [#22–2-109 to L.P.], NHMRC Investigator Grant [#2023/GNT2027049 to L.P.], MS Australia Incubator Grant [#19–0746 to L.P. and M.B.], and National Institutes of Health (U01AG072464). Spatial transcriptomics for this study was generously supported by the Just-In-Time (JIT) Core Usage Funding Program from the Institute of Clinical and Translational Sciences at Washington University in St. Louis and 10X genomics.

Data availability
The spatial Visium count matrices and processed data generated for this study are uploaded to the Synapse portal and can be accessed online through Synapse ID [syn69902953] (https://www.synapse.org/Synapse:syn69902953). The sequencing data is available for general research use with controlled access. Requests to access the sequencing data should be directed to the corresponding authors. Custom preprocessing and downstream analysis scripts required to reproduce the manuscript results are available at the Zenodo portal: https://zenodo.org/records/17184169

Declarations

Ethics approval and consent to participate
The Human Ethics Committee at the University of Sydney for acquiring control and MS tissue Sections (2020/HE000149).

Consent for publication
All authors have provided consent for publication.

Competing interest
The authors declare no competing interests.

Author details
[1]Charles Perkins Centre, Neuroscience, School of Medical Sciences, Faculty of Medicine and Health, University of Sydney, Sydney, NSW, Australia
[2]Division of Neurogenetics, Neurobiology of Aging and Resilience Centre, Ohio State University, Columbus, OH 43210, USA
[3]Department of Neurology, Washington University in St. Louis, St. Louis, MO 63110, USA
[4]Department of Neuropathology, Royal Prince Alfred Hospital, Sydney, NSW, Australia
[5]Brain and Mind Centre, University of Sydney, Sydney, NSW, Australia

Received: 19 January 2026 / Accepted: 23 January 2026
Published online: 16 February 2026

References

1. Kuhlmann T, Ludwin S, Prat A, Antel J, Brück W, Lassmann H (2017) An updated histological classification system for multiple sclerosis lesions. Acta Neuropathol 133:13–24. https://doi.org/10.1007/s00401-016-1653-y
2. Prineas JW, Lee S (2023) Microglia subtypes in acute, subacute, and chronic multiple sclerosis. J Neuropathol Exp Neurol 82:674–694. https://doi.org/10.1093/jnen/nlad046
3. Dal-Bianco A, Grabner G, Kronnerwetter C, Weber M, Höftberger R, Berger T et al (2017) Slow expansion of multiple sclerosis iron rim lesions: pathology and 7 T magnetic resonance imaging. Acta Neuropathol. https://doi.org/10.1007/s00401-016-1636-z
4. Absinta M, Sati P, Masuzzo F, Nair G, Sethi V, Kolb H et al (2019) Association of chronic active multiple sclerosis lesions with disability in vivo. JAMA Neurol. https://doi.org/10.1001/jamaneurol.2019.2399
5. Klotz L, Smolders J, Lehto J, Matilainen M, Lütje L, Buchholz L et al (2025) Broad rim lesions are a new pathological and imaging biomarker for rapid disease progression in multiple sclerosis. Nat Med 31:2016. https://doi.org/10.1038/S41591-025-03625-7
6. Prinz M, Masuda T, Wheeler MA, Quintana FJ (2021) Microglia and central nervous system-associated macrophages–from origin to disease modulation. Annu Rev Immunol. https://doi.org/10.1146/annurev-immunol-093019-110159
7. Vogel DYS, Vereyken EJF, Glim JE, Heijnen PDAM, Moeton M, van der Valk P et al (2013) Macrophages in inflammatory multiple sclerosis lesions have an intermediate activation status. J Neuroinflamm [Internet] 10:1–12. https://doi.org/10.1186/1742-2094-10-35/TABLES/3
8. Deczkowska A, Keren-Shaul H, Weiner A, Colonna M, Schwartz M, Amit I, Cell Press (2018) Disease-associated microglia: a universal immune sensor of neurodegeneration. Cell. https://doi.org/10.1016/j.cell.2018.05.003
9. Krasemann S, Madore C, Cialic R, Baufeld C, Calcagno N, El Fatimy R et al (2017) The TREM2-APOE pathway drives the transcriptional phenotype of dysfunctional microglia in neurodegenerative diseases. Immunity. https://doi.org/10.1016/j.immuni.2017.08.008
10. Cantoni C, Bollman B, Licastro D, Xie M, Mikesell R, Schmidt R et al (2015) TREM2 regulates microglial cell activation in response to demyelination in vivo. Acta Neuropathol 129:429–447. https://doi.org/10.1007/s00401-015-1388-1
11. Poliani PL, Wang Y, Fontana E, Robinette ML, Yamanishi Y, Gilfillan S et al (2015) TREM2 sustains microglial expansion during aging and response to demyelination. J Clin Invest 125:2161–2170. https://doi.org/10.1172/JCI77983
12. Cignarella F, Filipello F, Bollman B, Cantoni C, Locca A, Mikesell R et al (2020) TREM2 activation on microglia promotes myelin debris clearance and remyelination in a model of multiple sclerosis. Acta Neuropathol 140:513–534. https://doi.org/10.1007/s00401-020-02193-z
13. Takahashi K, Prinz M, Stagi M, Chechneva O, Neumann H (2007) TREM2-transduced myeloid precursors mediate nervous tissue debris clearance and facilitate recovery in an animal model of multiple sclerosis. PLoS Med 4:e124. https://doi.org/10.1371/JOURNAL.PMED.0040124
14. Hou J, Magliozzi R, Chen Y, Wu J, Wulf J, Strout G et al (2025) Acute TREM2 inhibition depletes MAFB-high microglia and hinders remyelination. Proc Natl Acad Sci U S A. https://doi.org/10.1073/pnas.2426786122
15. Wei W, Zhang L, Xin W, Pan Y, Tatenhorst L, Hao Z et al (2024) TREM2 regulates microglial lipid droplet formation and represses post-ischemic brain injury. Biomed Pharmacother 170:115962. https://doi.org/10.1016/J.BIOPHA.2023.115962
16. Nguyen TB, Louie SM, Daniele JR, Tran Q, Dillin A, Zoncu R et al (2017) DGAT1-dependent lipid droplet biogenesis protects mitochondrial function during starvation-induced autophagy. Dev Cell 42:9-21.e5. https://doi.org/10.1016/j.devcel.2017.06.003
17. Gouna G, Klose C, Bosch-Queralt M, Liu L, Gokce O, Schifferer M et al (2021) TREM2-dependent lipid droplet biogenesis in phagocytes is required for remyelination. J Exp Med 218:e20210227. https://doi.org/10.1084/JEM.20210227
18. Conte M, Medici V, Malagoli D, Chiariello A, Cirrincione A, Davin A et al (2022) Expression pattern of perilipins in human brain during aging and in Alzheimer's disease. Neuropathol Appl Neurobiol 48:e12756. https://doi.org/10.1111/nan.12756
19. Deming Y, Filipello F, Cignarella F, Cantoni C, Hsu S, Mikesell R et al (2019) The MS4A gene cluster is a key modulator of soluble TREM2 and Alzheimer's disease risk. Sci Transl Med. https://doi.org/10.1126/scitranslmed.aau2291
20. Silva-Gomes R, Mapelli SN, Boutet M-A, Mattiola I, Sironi M, Grizzi F et al (2022) Differential expression and regulation of MS4A family members in myeloid cells in physiological and pathological conditions. J Leukoc Biol 111:817–836. https://doi.org/10.1002/JLB.2A0421-200R
21. Li Y, Shen Z, Chai Z, Zhan Y, Zhang Y, Liu Z et al (2023) Targeting MS4A4A on tumour-associated macrophages restores CD8+ T-cell-mediated antitumour immunity. Gut 72:2307–2320. https://doi.org/10.1136/gutjnl-2022-329147
22. Jiang M, Li Q, Chen J, Li R, Yao J, Hu Y et al (2025) Microglial MS4A4A protects against epileptic seizures in Alzheimer's disease. Adv Sci. https://doi.org/10.1002/advs.202417733
23. You S-F, Brase L, Filipello F, Iyer AK, Del-Aguila J, He J et al (2023) MS4A4A modifies the risk of Alzheimer disease by regulating lipid metabolism and immune response in a unique microglia state. MedRxiv. https://doi.org/10.1101/2023.02.06.23285545
24. Danhash EP, Verbeck AC, Western D, Díaz-Pacheco AS, Galasso G, You S et al (2025) Ms4a4a deficiency ameliorates plaque pathology in a mouse model of amyloid accumulation. Alzheimers Dement 21:e70580. https://doi.org/10.1002/ALZ.70580
25. Koning N, Bö L, Hoek RM, Huitinga I (2007) Downregulation of macrophage inhibitory molecules in multiple sclerosis lesions. Ann Neurol. https://doi.org/10.1002/ana.21220
26. Piccio L, Buonsanti C, Cella M, Tassi I, Schmidt RE, Fenoglio C et al (2008) Identification of soluble TREM-2 in the cerebrospinal fluid and its association with multiple sclerosis and CNS inflammation. Brain 131:3081–3091. https://doi.org/10.1093/brain/awn217
27. Kiernan JA (1984) Chromoxane cyanine R. II. Staining of animal tissues by the dye and its iron complexes. J Microsc 134:25–39. https://doi.org/10.1111/j.1365-2818.1984.tb00501.x
28. Hao Y, Hao S, Andersen-Nissen E, Mauck WM, Zheng S, Butler A et al (2021) Integrated analysis of multimodal single-cell data. Cell 184:3573-3587.e29. https://doi.org/10.1016/j.cell.2021.04.048
29. Jäkel S, Agirre E, Mendanha Falcão A, van Bruggen D, Lee KW, Knuesel I et al (2019) Altered human oligodendrocyte heterogeneity in multiple sclerosis. Nature 566:543–547. https://doi.org/10.1038/s41586-019-0903-2
30. Franjic D, Skarica M, Ma S, Arellano JI, Tebbenkamp ATN, Choi J et al (2022) Transcriptomic taxonomy and neurogenic trajectories of adult human, macaque, and pig hippocampal and entorhinal cells. Neuron 110:452-469.e14. https://doi.org/10.1016/j.neuron.2021.10.036
31. Kleshchevnikov V, Shmatko A, Dann E, Aivazidis A, King HW, Li T et al (2022) Cell2location maps fine-grained cell types in spatial transcriptomics. Nat Biotechnol 40:661–671. https://doi.org/10.1038/s41587-021-01139-4
32. Absinta M, Maric D, Gharagozloo M, Garton T, Smith MD, Jin J et al (2021) A lymphocyte–microglia–astrocyte axis in chronic active multiple sclerosis. Nature 597:709–714. https://doi.org/10.1038/s41586-021-03892-7
33. Morabito S, Reese F, Rahimzadeh N, Miyoshi E, Swarup V (2023) HdWGCNA identifies co-expression networks in high-dimensional transcriptomics data. Cell Rep Methods 3:100498. https://doi.org/10.1016/j.crmeth.2023.100498
34. Kuleshov MV, Jones MR, Rouillard AD, Fernandez NF, Duan Q, Wang Z et al (2016) Enrichr: a comprehensive gene set enrichment analysis web server 2016 update. Nucleic Acids Res 44:W90–W97. https://doi.org/10.1093/nar/gkw377
35. Gao YH, Li X (2023) Cholesterol metabolism: towards a therapeutic approach for multiple sclerosis. Neurochem Int. https://doi.org/10.1016/j.neuint.2023.105501
36. Diaz-Lucena D, Kruse N, Thüne K, Schmitz M, Villar-Piqué A, da Cunha JEG et al (2021) Trem2 expression in the brain and biological fluids in prion diseases. Acta Neuropathol 141:841–859. https://doi.org/10.1007/s00401-021-02296-1
37. Lue LF, Schmitz CT, Serrano G, Sue LI, Beach TG, Walker DG (2015) Trem2 protein expression changes correlate with Alzheimer's disease neurodegenerative pathologies in post-mortem temporal cortices. Brain Pathol. https://doi.org/10.1111/bpa.12190
38. Jäckle K, Zeis T, Schaeren-Wiemers N, Junker A, van der Meer F, Kramann N et al (2020) Molecular signature of slowly expanding lesions in progressive multiple sclerosis. Brain. https://doi.org/10.1093/brain/awaa158
39. Zrzavy T, Hametner S, Wimmer I, Butovsky O, Weiner HL, Lassmann H (2017) Loss of 'homeostatic' microglia and patterns of their activation in active multiple sclerosis. Brain 140:1900–1913. https://doi.org/10.1093/BRAIN/AWX113
40. Alsema AM, Wijering MHC, Miedema A, Kotah JM, Koster M, Rijnsburger M et al (2024) Spatially resolved gene signatures of white matter lesion progression in multiple sclerosis. Nat Neurosci 27:2341–2353. https://doi.org/10.1038/s41593-024-01765-6
41. Lerma-Martin C, Badia-i-Mompel P, Ramirez Flores RO, Sekol P, Schäfer PSL, Riedl CJ et al (2024) Cell type mapping reveals tissue niches and interactions

in subcortical multiple sclerosis lesions. Nat Neurosci 27:2354–2365. https://doi.org/10.1038/s41593-024-01796-z
42. Horan K, Williams AC (2024) Mapping out multiple sclerosis with spatial transcriptomics: degenerative diseases. Nat Neurosci Nat Res. https://doi.org/10.1038/s41593-024-01798-x
43. Li Z, Chen R, Li Y, Zhou Q, Zhao H, Zeng K et al (2023) A comprehensive overview of PPM1B: from biological functions to diseases. Eur J Pharmacol 947:175633. https://doi.org/10.1016/J.EJPHAR.2023.175633
44. Mela A, Goldman JE (2009) The tetraspanin KAI1/CD82 is expressed by late-lineage oligodendrocyte precursors and may function to restrict precursor migration and promote oligodendrocyte differentiation and myelination. J Neurosci 29:11172–11181. https://doi.org/10.1523/JNEUROSCI.3075-09.2009
45. Suo N, Ye G, He B, Gu H, Xie X (2019) Inhibition of MAPK/ERK pathway promotes oligodendrocytes generation and recovery of demyelinating diseases. Glia [Internet] 67:1320. https://doi.org/10.1002/GLIA.23606
46. Hoi KK, Xia W, Wei MM, Ulloa Navas MJ, Garcia Verdugo JM, Nachury MV et al (2023) Primary cilia control oligodendrocyte precursor cell proliferation in white matter injury via Hedgehog-independent CREB signaling. Cell Rep 42:113272. https://doi.org/10.1016/J.CELREP.2023.113272
47. Ki SM, Jeong HS, Lee JE (2021) Primary cilia in glial cells: an oasis in the journey to overcoming neurodegenerative diseases. Front Neurosci. https://doi.org/10.3389/fnins.2021.736888
48. Serafini B, Rosicarelli B, Magliozzi R, Stigliano E, Capello E, Mancardi GL et al (2006) Dendritic cells in multiple sclerosis lesions: maturation stage, myelin uptake, and interaction with proliferating T cells. J Neuropathol Exp Neurol 65:124–141. https://doi.org/10.1097/01.jnen.0000199572.96472.1c
49. Hofmann A, Krajnc N, Dal-Bianco A, Riedl CJ, Zrzavy T, Lerma-Martin C et al (2023) Myeloid cell iron uptake pathways and paramagnetic rim formation in multiple sclerosis. Acta Neuropathol 146(5):707. https://doi.org/10.1007/S00401-023-02627-4
50. Zhang Z, Zhang ZY, Schittenhelm J, Wu Y, Meyermann R, Schluesener HJ (2011) Parenchymal accumulation of CD163+ macrophages/microglia in multiple sclerosis brains. J Neuroimmunol 237:73–79. https://doi.org/10.1016/j.jneuroim.2011.06.006
51. Zheng L, Guo Y, Zhai X, Zhang Y, Chen W, Zhu Z et al (2022) Perivascular macrophages in the CNS: from health to neurovascular diseases. CNS Neurosci Ther 28:1908–1920. https://doi.org/10.1111/CNS.13954
52. Morgan BP, Gommerman JL, Ramaglia V (2021) An "Outside-in" and "Inside-out" consideration of complement in the multiple sclerosis brain: lessons from development and neurodegenerative diseases. Front Cell Neurosci. https://doi.org/10.3389/fncel.2020.600656
53. Lassmann H (2019) Pathogenic mechanisms associated with different clinical courses of multiple sclerosis. Front Immunol. https://doi.org/10.3389/fimmu.2018.03116
54. Van Gorp H, Delputte PL, Nauwynck HJ (2010) Scavenger receptor CD163, a jack-of-all-trades and potential target for cell-directed therapy. Mol Immunol 47:1650–1660. https://doi.org/10.1016/j.molimm.2010.02.008
55. Kessler W, Thomas C, Kuhlmann T (2023) Microglia activation in periplaque white matter in multiple sclerosis depends on age and lesion type, but does not correlate with oligodendroglial loss. Acta Neuropathol 146:817. https://doi.org/10.1007/S00401-023-02645-2
56. Robichaud S, Fairman G, Vijithakumar V, Mak E, Cook DP, Pelletier AR et al (2021) Identification of novel lipid droplet factors that regulate lipophagy and cholesterol efflux in macrophage foam cells. Autophagy 17:3671–3689. https://doi.org/10.1080/15548627.2021.1886839
57. Yang D, Wang X, Zhang L, Fang Y, Zheng Q, Liu X et al (2022) Lipid metabolism and storage in neuroglia: role in brain development and neurodegenerative diseases. Cell Biosci 12:106. https://doi.org/10.1186/S13578-022-00828-0
58. Yang J, Wu J, Xie X, Xia P, Lu J, Liu J et al (2025) Perilipin-2 mediates ferroptosis in oligodendrocyte progenitor cells and myelin injury after ischemic stroke. Neural Regen Res 20:2015–2028. https://doi.org/10.4103/NRR.NRR-D-23-01540
59. Marschallinger J, Iram T, Zardeneta M, Lee SE, Lehallier B, Haney MS et al (2020) Lipid-droplet-accumulating microglia represent a dysfunctional and proinflammatory state in the aging brain. Nat Neurosci 23(2):194–208. https://doi.org/10.1038/S41593-019-0566-1
60. Lee CH, Kim HJ, Lee YS, Kang GM, Lim HS, Lee S et al (2018) Hypothalamic macrophage inducible nitric oxide synthase mediates obesity-associated hypothalamic inflammation. Cell Rep 25:934-946.e5. https://doi.org/10.1016/j.celrep.2018.09.070
61. Lin M, Yu JX, Zhang WX, Lao FX, Huang HC (2024) Roles of TREM2 in the pathological mechanism and the therapeutic strategies of Alzheimer's disease. J Preve Alzheimer's Dis 11:1682. https://doi.org/10.14283/JPAD.2024.164
62. Shao G, Cui X, Wang Y, Luo S, Li C, Jiang Y et al (2024) Targeting MS4A4A: a novel pathway to improve immunotherapy responses in glioblastoma. CNS Neurosci Ther. https://doi.org/10.1111/cns.14791
63. Rosner D, Sun J, Yee A, Wagh C, Rychkova A, Cacace R et al (2024) The Alzheimer's disease risk genes MS4A4A And MS4A6A cooperate to negatively regulate Trem2 and Microglia states. Neuron. https://doi.org/10.1101/2024.11.23.625001

Publisher's Note